International Journal of Biological Macromolecules

SERICIN-REINFORCED POLYSACCHARIDE COMPOSITES FOR POTENTIAL REGENERATIVE AND ANTIBACTERIAL APPLICATIONS

--Manuscript Draft--

Manuscript Number:	IJBIOMAC-D-25-21651R3
Article Type:	Research Paper
Section/Category:	Carbohydrates, Natural Polyacids and Lignins
Keywords:	biomaterials; drug delivery; antibacterial activity
Corresponding Author:	Barbara Kołodziejska, Ph.D. Medical University of Warsaw POLAND
First Author:	Barbara Kołodziejska, Ph.D.
Order of Authors:	Barbara Kołodziejska, Ph.D.
	Andrzej Pyzik
	Ramona Figat, Ph.D.
	Julia Kopczyńska
	Magdalena Kowalczyk, Prof.
	Joanna Kolmas, Prof.
Abstract:	In this work, three polysaccharide matrices were prepared with varying chitosan-to-alginate weight ratios (70:30, 50:50, 30:70) and used to develop sericin-reinforced composite biomaterials loaded with ciprofloxacin and silver, either as nanoparticles or silver ions incorporated into nanocrystalline hydroxyapatite (AgHA). To obtain composites, a solid-liquid method was employed in combination with lyophilization. SEM analysis revealed highly porous structures with pore sizes ranging from 50 to 200 μm for silver nanoparticle composites and below 100 μm for AgHA-containing composites. Ciprofloxacin was loaded with high efficiency (95.2±1.1%), while silver loading efficiencies were 29.3±2.6% for nanoparticles and 20.4±1.3% for AgHA. In vitro release studies demonstrated biphasic ciprofloxacin release over 28 days, with initial diffusion-driven release followed by a slower phase (Korsmeyer-Peppas model, n = 0.035–0.070). Silver ions were released similarly, whereas silver nanoparticles exhibited zero-order kinetics in the second phase. Antimicrobial testing revealed significant activity against multi-drug-resistant Staphylococcus aureus NCTC9789 and Pseudomonas aeruginosa PAO1161. Cytotoxicity assays confirmed that all composites were non-toxic to BALB/c 3T3 fibroblasts. These results indicate that the developed composites possess dual functionality—serving as temporary bone dressings for wounds and local drug delivery systems—offering sustained antibiotic release and prolonged antimicrobial protection, which may help to prevent infections associated with orthopedic implants.
Opposed Reviewers:	
Response to Reviewers:	

Medical University of Warsaw
Faculty of Pharmacy
Department of Pharmaceutical Chemistry and Biomaterials
ul. Banacha 1, 02-097 Warsaw, Poland

Barbara Kołodziejska, PhD E-mail: barbara.kolodziejska@wum.edu.pl

Warsaw, 5th of January 2026

Prof. Jayaramudu Tippabattini
Editor
International Journal of Biological Macromolecules

Dear Professor Tippabattini,

I am pleased to resubmit the revised version of our manuscript entitled **"SERICIN-REINFORCED POLYSACCHARIDE COMPOSITES FOR POTENTIAL REGENERATIVE AND ANTIBACTERIAL APPLICATIONS"** (Manuscript No. IJBIOMAC-D-25-21651R3) for further consideration in *International Journal of Biological Macromolecules*.

We are sincerely grateful for the time and effort dedicated by the Reviewers and by you in evaluating our work. The constructive comments received during the third review round—particularly the detailed minor suggestions from Reviewer 1—were helpful in further improving the clarity, precision, and overall quality of our manuscript. We have carefully addressed every point raised and incorporated all recommended modifications. We also responded comment provided by Reviewer 4.

A detailed, point-by-point response to all Reviewer comments is included in the accompanying file.

We believe that the manuscript has been substantially strengthened following all rounds of revision and now presents the results of our study with significantly improved clarity and scientific rigor. We confirm that the manuscript is original, has not been published or submitted elsewhere, and that all authors have approved the final version.

We would like to express our sincere gratitude once again for your time, guidance, and constructive feedback throughout the review process. We hope that the revised manuscript will now be suitable for publication in *International Journal of Biological Macromolecules*.

Yours sincerely,

Barbara Kołodziejska

Reviewer #1

The authors are grateful for all the remarks and the possibility to response to them. In reply, the following document was prepared. The appropriate changes in the text were made and highlighted with a red color. Short comments, explanations and responses to the remarks, which were not placed in the main text, were highlighted with a blue color.

1. Are the objectives and the rationale of the study clearly stated? If no, please provide comments and suggestions for improvements in the comment to the authors (in point 11).

Reviewer #1: Yes

2. Please rate the novelty of the findings – on a scale of 1 (lowest novelty) to 10 (highest novelty).

Reviewer #1: 7

3. If applicable, is the method/study reported in sufficient detail to allow for its replicability and/or reproducibility? If no, please provide comments and suggestions for improvements in the comment to the authors (in point 11)

Reviewer #1: Yes

4. If applicable, are the statistical analyses, controls, sampling mechanisms, and statistical reporting (e.g., P-values, confidence intervals, effect sizes) appropriate and well described? If no, please provide comments and suggestions for improvements in the comment to the authors (in point 11)

Reviewer #1: Yes

5. Could the manuscript benefit from additional tables or figures, or from improving or removing some of the existing ones? If yes, please provide comments and suggestions for improvements in the comment to the authors (in point 11)

Reviewer #1: No

6. If applicable, are the interpretation of the results and the study conclusions supported by the data? If no, please provide comments and suggestions for improvements in the comment to the authors (in point 11)

Reviewer #1: Yes

7. Have the authors clearly emphasized the strengths of their study/methods? If no, please provide comments and suggestions for improvements in the comment to the authors (in point 11)

Reviewer #1: Yes

8. Have the authors clearly acknowledged the limitations of their study/methods? If no, please provide comments and suggestions for improvements in the comment to the authors (in point 11)

Reviewer #1: Yes

9. Does the manuscript's structure, flow, or writing style require improvement (e.g., addition of subheadings, shortening of text, reorganization of sections, or relocating details)? If yes, please provide comments and suggestions for improvements in the comment to the authors (in point 11)

Reviewer #1: No

10. Could the manuscript benefit from language editing?

Reviewer #1: No

Reviewer #1: A manuscript is significantly improved; however, the following few concerns should be clarified for it to be accepted.

1. An equation for the swelling ratio should be written properly using the equation editor; remove % in "100%" and all equations should be numerically numbered.

Thank you for this valuable comment. The equation for the swelling ratio has been revised using the equation editor, the percentage symbol in “100%” has been removed, and all equations in the manuscript have now been numbered sequentially.

To calculate the swelling ratio at time t, the following equation was used:

$$\%SR = \frac{(W_t - W_0)}{W_0} \times 100 \qquad (1)$$

2. Figure 3c & d "representative model fittings....." which model?. Please specify.

Thank you for this helpful comment. The figure caption has been revised to explicitly specify the model used. It now states that the representative fittings correspond to the Korsmeyer–Peppas model for C3AgHA in both the short- and long-term release ranges (Figure 3c and d, respectively).

Figure 3. Ciprofloxacin release profiles from the composite matrices: full release curves over 672 hours (a), initial release phase - first 48 hours (b); representative model fittings to Korsmeyer-Peppas model for C3AgHA in the short- and long-term release ranges (c, d – respectively).

3. In table 2, remove the quotation marks in the word "Zero"

Thank you for pointing this out. The quotation marks around the word Zero in Table 2 have been removed as suggested.

	Ciprofloxacin release							
Sample	I phase (0-48 hours)				II phase (48-672 hours)			
	k_{KP}	n	R^2	Model	k_{KP}	n	R^2	model
C1AgHA	8.7±0.4	0.14±0.01	0.9840	K-P	12.5±0.1	0.036±0.001	0.9955	K-P
C2AgHA	7.1±0.5	0.23±0.02	0.9831	K-P	13.4±0.1	0.048±0.002	0.9975	K-P
C3AgHA	9.4±0.6	0.22±0.02	0.9833	K-P	18.3±0.2	0.040±0.002	0.9947	K-P
C1Ag-n	15.0±0.9	0.19±0.02	0.9799	K-P	26.5±0.2	0.035±0.001	0.9980	K-P
C2Ag-n	15.4±0.9	0.23±0.02	0.9868	K-P	28.5±0.2	0.070±0.001	0.9996	K-P
C3Ag-n	13.6±0.8	0.23±0.02	0.9877	K-P	27.9±0.3	0.051±0.002	0.9982	K-P
	Ag release							
	I phase (0-48 hours)				II phase (48-672 hours)			
C1AgHA	6.0±0.4	0.17±0.02	0.9604	K-P	8.8±0.3	0.058±0.005	0.9885	K-P
C2AgHA	1.04±0.04	0.23±0.02	0.9905	K-P	1.6±0.2	0.14±0.02	0.9627	K-P
C3AgHA	2.2±0.1	0.27±0.02	0.9850	K-P	4.1±0.2	0.107±0.007	0.9944	K-P
					Q_0	k	R^2	
C1Ag-n	1.06±0.04	0.24±0.01	0.9921	K-P	2.16±0.06	0.012±0.001	0.9998	Zero order
C2Ag-n	3.3±0.2	0.21±0.03	0.9671	K-P	7.2±0.2	0.0029±0.0004	0.9682	Zero order
C3Ag-n	1.64±0.08	0.28±0.02	0.9937	K-P	4.8±0.20	0.0154±0.0005	0.9984	Zero order

Reviewer #4

The authors are grateful for all the remarks and the possibility to response to them. In reply, the following document was prepared. The appropriate changes in the text were made and highlighted with a red color. Short comments, explanations and responses to the remarks, which were not placed in the main text, were highlighted with a blue color.

1. Are the objectives and the rationale of the study clearly stated? If no, please provide comments and suggestions for improvements in the comment to the authors (in point 11).

Reviewer #4: Yes

2. Please rate the novelty of the findings – on a scale of 1 (lowest novelty) to 10 (highest novelty).

Reviewer #4: 7

3. If applicable, is the method/study reported in sufficient detail to allow for its replicability and/or reproducibility? If no, please provide comments and suggestions for improvements in the comment to the authors (in point 11)

Reviewer #4: Yes

4. If applicable, are the statistical analyses, controls, sampling mechanisms, and statistical reporting (e.g., P-values, confidence intervals, effect sizes) appropriate and well described? If no, please provide comments and suggestions for improvements in the comment to the authors (in point 11)

Reviewer #4: Yes

5. Could the manuscript benefit from additional tables or figures, or from improving or removing some of the existing ones? If yes, please provide comments and suggestions for improvements in the comment to the authors (in point 11)

Reviewer #4: No

6. If applicable, are the interpretation of the results and the study conclusions supported by the data? If no, please provide comments and suggestions for improvements in the comment to the authors (in point 11)

Reviewer #4: Yes

7. Have the authors clearly emphasized the strengths of their study/methods? If no, please provide comments and suggestions for improvements in the comment to the authors (in point 11)

Reviewer #4: Yes

8. Have the authors clearly acknowledged the limitations of their study/methods? If no, please provide comments and suggestions for improvements in the comment to the authors (in point 11)

Reviewer #4: Yes

9. Does the manuscript's structure, flow, or writing style require improvement (e.g., addition of subheadings, shortening of text, reorganization of sections, or relocating details)? If yes, please provide comments and suggestions for improvements in the comment to the authors (in point 11)

Reviewer #4: No

10. Could the manuscript benefit from language editing?

Reviewer #4: No

Reviewer #4: All the comments have been addressed successfully but still there are some minor issues are need to be addressed. Those can be corrected during proofreading and the manuscript can be accepted in the present form.

We thank the Reviewer for the positive evaluation of the revised manuscript. In addition to addressing all major comments, we have also carefully considered and incorporated the minor remarks from the previous review, which helped us further refine the manuscript and identify additional minor issues. These have been corrected accordingly, and any remaining minor points can be addressed during the proofreading stage.

SERICIN-REINFORCED POLYSACCHARIDE COMPOSITES FOR POTENTIAL REGENERATIVE AND ANTIBACTERIAL APPLICATIONS

Barbara Kołodziejska[1*], Andrzej Pyzik[1], Ramona Figat[2], Julia Kopczyńska[3], Magdalena Kowalczyk[3], Joanna Kolmas[1]

[1]Department of Pharmaceutical Chemistry and Biomaterials, Faculty of Pharmacy, Medical University of Warsaw, Banacha 1 str., 02-097, Warsaw, Poland

[2]Department of Toxicology and Bromatology, Faculty of Pharmacy, Medical University of Warsaw, Banacha 1 str., 02-097, Warsaw, Poland

[3]Institute of Biochemistry and Biophysics, Polish Academy of Sciences, Pawińskiego 5A, 02-106 Warsaw, Poland

[*]**Corresponding Author**

Barbara Kołodziejska

Medical University of Warsaw

Faculty of Pharmacy

Department of Pharmaceutical Chemistry

ul. Banacha 1, 02-097 Warsaw, Poland.

Phone: +48 22 5720755

e-mail: barbara.kolodziejska@wum.edu.pl

Abstract

In this work, three polysaccharide matrices were prepared with varying chitosan-to-alginate weight ratios (70:30, 50:50, 30:70) and used to develop sericin-reinforced composite biomaterials loaded with ciprofloxacin and silver, either as nanoparticles or silver ions incorporated into nanocrystalline hydroxyapatite (AgHA). To obtain composites, a solid-liquid method was employed in combination with lyophilization. SEM analysis revealed highly porous structures with pore sizes ranging from 50 to 200 μm for silver nanoparticle composites and below 100 μm for AgHA-containing composites. Ciprofloxacin was loaded with high efficiency (95.2±1.1%), while silver loading efficiencies were 29.3±2.6% for nanoparticles and 20.4±1.3% for AgHA. In vitro release studies demonstrated biphasic ciprofloxacin release over 28 days, with initial diffusion-driven release followed by a slower phase (Korsmeyer-Peppas model, n = 0.035–0.070). Silver ions were released similarly, whereas silver nanoparticles exhibited zero-order kinetics in the second phase. Antimicrobial testing revealed significant activity against multidrug-resistant Staphylococcus aureus NCTC9789 and Pseudomonas aeruginosa PAO1161. Cytotoxicity assays confirmed that all composites were non-toxic to BALB/c 3T3 fibroblasts. These results indicate that the developed composites possess dual functionality—serving as temporary bone dressings for wounds and local drug delivery systems—offering sustained antibiotic release and prolonged antimicrobial protection, which may help to prevent infections associated with orthopedic implants.

Keywords: biomaterials, drug delivery, antibacterial activity, ciprofloxacin, composite

Introduction

Peri-implant infections, also known as Biomaterial-Associated Infections (BAIs), remain a significant challenge in reconstructive and restorative surgery, including dental and bone implantology, despite numerous preventive measures [1]. Bacterial colonisation of biomaterial surfaces, which initiates infection, can disrupt the functional integration of the biomaterial with bone tissue. The inflammation induced by the infection leads to resorption of the bone tissue surrounding the implant, ultimately resulting in poor implant-to-tissue integration and implant loss. A particularly challenging aspect of these infections is the formation of biofilms by bacteria, which confer significant resistance to many bactericidal agents. Systemic prophylactic antibiotic therapy is not always effective, largely due to poor drug penetration into inflamed, hypoxic tissues. Consequently, strategies such as intraoperative localised antibiotic administration are actively explored for more effective prevention [2,3].

The development of new antibiotics and antibacterial agents is a key priority for the World Health Organization (WHO) [4]. At the same time, traditional solutions, such as silver ions and nanoparticles, are being revisited due to their potent antibacterial activity. The antibacterial efficacy of silver has been recognised since antiquity, with no reports of bacterial resistance to date. Silver is currently being investigated for its effectiveness in treating infections caused by multidrug-resistant bacterial strains [5–8]. The bactericidal mechanism of silver involves interactions between silver ions and thiol (-SH) groups in bacterial proteins, leading to the substitution of hydrogen atoms and the formation of S-Ag bonds. This results in protein denaturation, deactivation of cellular pumps, membrane dysfunction, and the destruction of bacterial cell walls and membranes [6,9].

In bone tissue engineering, the current focus includes developing biomaterials, that not only fill bone defects or replace degraded tissue but also serve as carriers for drug delivery, such as antibiotics. Composite materials are particularly promising in fulfilling these dual roles and

offering appropriate biocompatibility, mechanical strength, enhanced tissue-implant integration, and prolonged, effective drug release [10–12].

Over the past two decades, significant attention has been directed towards materials of natural origin, including natural polymers, for composite development. Among these, alginate and chitosan have been extensively studied [13–20].

Chitosan, a linear polymer composed of randomly distributed β-(1,4)-D-glucosamine and N-acetyl-D-glucosamine units, commercially produced by deacetylation of chitin, a major component of crustacean exoskeletons and fungal cell walls. Chitosan exhibits excellent biocompatibility, biodegradability, and non-toxicity. Its chemical structure, particularly the presence of protonable amino groups along the D-glucosamine residues, accounts for most of its biological properties. These positively charged groups interact with negatively charged cell membranes, conferring hemostatic, mucoadhesive, antibacterial, and antifungal properties. Furthermore, chitosan's absorption capacity and ability to form porous, fibrous scaffolds make it suitable for controlled drug delivery systems and sustained-release applications [21,22].

Alginate, a biodegradable linear copolymer of β-D-mannuronate and α-L-guluronate molecules linked by β-1,4-glycosidic bonds, is primarily derived from seaweed and marine algae (e.g., *Laminaria hyperborea* and *Macrocystis pyrifera*). Alginic acid and its sodium salt form durable gels upon cross-linking with divalent cations, a property widely used in biomaterial engineering and medicine [23]. The hydrophilic nature of alginate gels makes them effective as wound dressings, capable of absorbing exudates and accelerating healing. Numerous studies highlight alginates' potential as carriers for controlled drug release [24].

In inorganic-organic bone composites, hydroxyapatite ($Ca_{10}(PO_4)_6(OH)_2$) is the most commonly used inorganic component. This material closely resembles biological apatite in composition and structure, a key component of the inorganic matrix in mineralised tissues (e.g., enamel,

dentin, and bone) [25–27]. Nanocrystalline hydroxyapatite offers excellent biocompatibility, osteoconductivity, non-toxicity, and immunogenicity, making it an exceptional bone substitute material with high potential for use as a drug delivery vehicle for direct application to bone tissue [28,29].

Our composites were reinforced with sericin, a globular protein present in silk produced by the *Bombyx mori* silkworm. Sericin contains numerous polar groups, enabling interactions with other polymers to improve mechanical properties and enhance the stability of biomaterials. Moreover, numerous studies have shown that sericin accelerates wound healing and collagen production with minimal immune response [30–33]. It also has a bactericidal effect and effectively inhibits the development of biofilm [34–36]. In osteoblast studies, sericin increased their proliferation and demonstrated regenerative effects on bone tissue [37–39].

Our research aimed to develop new polysaccharide composites reinforced with sericin, capable of releasing both the antibiotic and silver to ensure effective antibacterial activity. Until now, researchers worldwide have focused on developing biomaterials with a similar composition [40–43]; however, their primary objective was to design local wound dressings capable of delivering drugs with appropriate release kinetics. In contrast to these studies, our goal was to obtain a local dressing intended for application within bone tissue, which could be utilised in dentistry or for the treatment of minor bone defects, serving a preventive function by inhibiting the development of bacterial infections. It is of utmost importance to develop materials specifically targeted for bone tissue, as it is poorly vascularized; consequently, systemic pharmacotherapy is often insufficiently effective. We evaluated the efficacy of silver release in the form of nanoparticles and silver ions from Ag-substituted nanohydroxyapatite. The physicochemical properties of the composites were analysed, and the release profiles of both silver and antibiotic (ciprofloxacin) were examined. The antibacterial activity and cytotoxicity of the obtained materials were also studied.

Materials and Methods

Synthesis of hydroxyapatite containing silver ions (AgHA)

Hydroxyapatite containing silver ions was synthesized using the method described in detail by Pajor et al. [44]. Briefly, calcium nitrate tetrahydrate $Ca(NO_3)_2 \cdot 4H_2O$ (purity 99%) and silver nitrate ($AgNO_3$, assay ≥99.0%) were used as sources of calcium and silver ions, respectively, and were dissolved in distilled water. Then, an ammonium hydrogen phosphate solution ($(NH_4)_2HPO_4$, assay ≥98%) was introduced dropwise in such an amount that the (Ca+Ag)/P molar ratio was 1.67 and stirred on a magnetic stirrer. All the reagents were of analytical grade and purchased from Sigma Aldrich Chemicals, St. Louis, MO, USA. After mixing the solutions, a white precipitate formed. Then, the flasks with the suspension were left with the stirrer on for another 1 hour, and then the suspension was made alkaline with a 25% NH_4OH solution (≥99.99% trace metals basis), adjusting the pH to approximately 11. In the next stage, the mixing was turned off and the precipitate in the mother solution was left for 24 hours to age (so-called precipitate maturation). After 24 hours, the obtained apatites were centrifuged and rinsed several times with distilled water until the pH reached ~ 7. After centrifugation, the precipitate was filtered under reduced pressure and then dried at 100°C for 24 hours. After drying, the obtained precipitate was micronized using an agate mortar. Subsequently the powder was sieved through a <40 μm mesh to eliminate hard agglomerates and subjected to further tests. For comparison, the pure, unsubstituted hydroxyapatite (HA) was obtained in the same conditions.

The identity of the obtained powders was examined using the powder X-ray diffraction (PXRD) method. A Bruker D8 Discover diffractometer equipped with a position detector and Cu-Kα radiation (λ = 0.15418 nm) was used. The measurements used the horizontal Bragg–Brentano (θ/θ) geometry (plane reflection mode) in the range from 15° to 60° (2θ) in a continuous scan, using steps of 0.03° and 2 s/step (total time 384 s/step). The identification of crystalline phases

was obtained by comparing the obtained diffractograms of HA and Ag-HA samples with the standard reference (JCPDS 09-0432). The mid-infrared FT-IR spectroscopy method in the transmission technique (using a KBr pellet) was used to analyse the chemical structure of hydroxyapatites. FT-IR spectra were recorded on a Shimadzu spectrometer with a resolution of 2 cm^{-1}, in the 4000-400 cm^{-1} range. Each measurement was performed using 30 scans. The crystal morphology was analysed by transmission electron microscopy (TEM) using the high-performance JEM 1400 transmission electron microscope (TEM-JEOL Co., Tokyo, Japan, 2008), equipped with Morada G2 TEM camera (EMSIS GmbH, Germany) under an accelerating voltage of 80 kV. Sample preparation consisted of dropping a suspension of the tested powder previously prepared in ethanol onto a Formvar grid. The silver content of the hydroxyapatite sample enriched in silver ions was measured using the F-AAS method (ANALYST 400, Perkin Elmer, Llantrisant, UK, with detection at a wavelength of $\lambda = 328.07$ nm). For this purpose, the sample was dissolved in super-pure concentrated nitric acid (63% HNO_3) and appropriately diluted with deionized water. The calibration curve was prepared by dissolving an appropriate amount of calibration $AgNO_3$ standard in deionized water (Avantor Performance Materials, Gliwice, Poland).

Preparation of composites

To obtain composites, the following reagents were prepared: chitosan (medium molecular weight, 75–85% deacetylation degree, viscosity ≤ 300 cP, Sigma-Aldrich, Burlington, MO, USA), sodium alginate (Sigma Aldrich, Burlington, MO, USA), sericin from *Bombyx mori* (silkworm, Sigma Aldrich, Burlington, MO, USA), glycerin (Sigma Aldrich, Burlington, MO, USA), silver nanoparticles (5 nm particle size, 5 mg/mL, silver nanospheres, in 2mM aqueous sodium citrate, nanoComposix), and hydroxyapatite enriched with silver ions (AgHA). A 3 wt.% suspension of alginate and chitosan was prepared in distilled water and combined in three different weight ratios of 30:70, 50:50, and 70:30. To 80 mL of each mixture obtained in this

way, 8 drops (~0.4 mL) of pure glycerin (≥99.5%) and 1.0 mL of sericin solution was added (prepared by dissolving 0.1 g of *Bombyx mori* sericin powder in 1.0 mL of distilled water under gentle stirring to ensure complete dissolution). After thorough mixing, 3.6 g of AgHA or 0.4 mL of silver nanoparticle suspension was added (in both cases, the amount corresponded to 6 mg of silver per 1 gram of composite). Since no aggregation-inducing conditions were introduced during the composite preparation, the size of nanoparticles was assumed to remain comparable to that in the free form. Finally, 145 mg of ciprofloxacin was added to the obtained thick suspension (the amount corresponds to 100 mg of ciprofloxacin per 1 g of the composite). All obtained suspensions were poured into Petri dishes. Then the dishes were frozen at -80°C and lyophilised for 48h. Freeze-dried samples were cross-linked using first 1.5% $CaCl_2$ solution (cross-linking for 10 min) and then 1M NaOH solution (cross-linking for 10 min). After cross-linking, the samples were rinsed three times for 15 min in distilled water and subjected to freezing and lyophilisation again. The solutions obtained after cross-linking and rinsing were collected in tubes to determine the ciprofloxacin content released during cross-linking and rinsing. As a result of the above procedures, six different composites were obtained, differing in the alginate-to-chitosan ratio and the form of incorporated silver (nano-Ag and AgHA). The list of obtained samples is presented in Table 1.

Table 1. Types of obtained composites.

Sample	**C1AgHA**	**C1Ag-n**	**C2AgHA**	**C2Ag-n**	**C3AgHA**	**C3Ag-n**
Polymer ratio (alginate: chitosan)	**30:70** (24 mL of 3% alginate and 56 mL of 3% chitosan)		**70:30** (56 mL of 3% alginate and 24 mL of 3% chitosan)		**50:50** (40 mL of 3% alginate and 40 mL of 3% chitosan)	
Glycerin	0.4 mL	0.4 mL	0.4 mL	0.4 mL	0.4 mL	0.4 mL

Sericin	1.0 mL of 10% solution	1.0 mL of 10% solution	1.0 mL of 10% solution	1.0 mL of 10% solution	1.0 mL of 10% solution	1.0 mL of 10% solution
Hydroxyapatite doped with silver	3.6 g	-	3.6 g	-	3.6 g	-
Silver nanoparticles	-	0.4 mL of 5 mg/mL	-	0.4 mL of 5 mg/mL	-	0.4 mL of 5 mg/mL
Ciprofloxacin	145 mg	145 mg	145 mg	145 mg	145 mg	145 mg

Studies of the obtained composites

To assess the porosity and topographic structure of the surface of the obtained composites, the samples were examined by scanning electron microscopy (SEM, Nova NanoSEM 200, Fei).

The mid-infrared FT-IR spectroscopy method in the attenuated total reflectance (ATR-FTIR) technique was used to analyse the chemical structure of all composites. FT-IR spectra were recorded on a Shimadzu IRAffinity-1S spectrometer in the 4000–400 cm^{-1} range. Each measurement was performed using 150 scans.

The swelling test was performed using the standard gravimetric method. Firstly, the lyophilised samples were weighed (initial weight, W_0). Then, the samples were immersed in phosphate-buffered saline (PBS; pH 7.4) at 37 °C. At predetermined time intervals (15 minutes, 30 minutes, 1 hour, 3 hours, 5 hours, 12 hours, 24 hours and 48 hours) the samples were removed from the solution, wiped dry with filter paper to remove excess liquid from the surface, and weighed again.

To calculate the swelling ratio at time t, the following equation was used:

$$\%SR = \frac{(W_t - W_0)}{W_0} \times 100 \quad (1)$$

where W_0 and W_t are the weights of the initial dry and swollen samples at fixed time intervals t, respectively. All the measurements were performed in triplicate.

The study of ciprofloxacin and silver release from the obtained composites was carried out using the HPLC method and the F-AAS method, respectively. The prepared composite samples, in the form of cylindrical discs with a diameter of 15 mm, a height of 10 mm, and a mass of 300 mg were placed in falcon test tubes, to which 50 mL of distilled water was added. The test tubes were placed in a shaker and incubated at 37°C while slowly mixing to ensure conditions similar to physiological conditions. The shaking frequency was set at 50 rpm. Samples of the incubation media were taken first after 15 and 30 minutes, then after 1, 3, 6, 12, 24, 48 and 72 hours and then after 7, 14, 21 and 27 days. Before each collection, the contents of the test tubes were mixed thoroughly, then 10 mL of the solution was taken using a syringe, filtered into a new test tube using membrane filters and, finally, the test tubes with composite samples were filled with the same volume of distilled water. Ciprofloxacin release was studied using the HPLC method. Sample analysis was performed on an RP-18 column (HPLC Column 250 x 4.6 mm x 1/4'' Microsorb-MV 100-5 C18), which was thermostated in a CTO-10ASVP oven from Shimadzu. The analysis was performed in a reverse phase system, using a mixture of phosphate buffer with pH = 3 and acetonitrile in a volume ratio of 80:20 as the mobile phase. The eluent flow rate was 1 mL/min. The chromatograph was connected to a UV-Vis detector (Varian Prostar 325). Each time, 20 µl of the solution was introduced into the column. Before starting the sample measurements, a calibration curve was prepared using standard solutions. Absorbance was measured at a wavelength of 278 nm. To investigate the release profile of silver from the composites, the F-AAS method (PerkinElmer AAnalyst 400 AA Spectrometer) was used at a wavelength of 328 nm, after preparing a calibration curve.

To evaluate the release mechanism and kinetics of ciprofloxacin and silver, the experimental data were fitted to several mathematical models commonly used to describe drug release from polymeric and composite matrices.

Zero-order model:

$$\frac{Q_t}{Q_\infty} = k_0 t \quad (2)$$

First-order model:

$$\log(1 - \frac{Q_t}{Q_\infty}) = -k_1 t/2.303 \quad (3)$$

Higuchi model:

$$Q_t/Q_\infty = k_H t^{1/2} \quad (4)$$

Korsmeyer–Peppas model (K–P model):

$$\frac{Q_t}{Q_\infty} = k_{KP} t^n \quad (5)$$

Peppas–Sahlin model:

$$\frac{Q_t}{Q_\infty} = k_1 t^n + k_2 t^{2n} \quad (6)$$

Weibull model:

$$\frac{Q_t}{Q_\infty} = 1 - \exp[-(\frac{t-T_i}{\tau})^\beta] \quad (7)$$

Where k_0, k_1, k_2, k_H, k_{KP}, τ refer to the rate constants, Q_t/Q_∞ represents the fraction of the drug released at a time t, n refers to the diffusion coefficient, Ti - the lag time before release onset, and β is the shape parameter. Depending on the value of β, the release profile may be exponential ($\beta = 1$), parabolic ($\beta < 1$), or sigmoidal ($\beta > 1$) [45,46].

All models were fitted to the experimental data using nonlinear regression. The coefficient of determination (R^2) was used to evaluate the goodness of fit. Model equations and parameters were implemented in Kaleidagraph 5 (Synergy Software).

The cytotoxicity of the materials was evaluated in accordance with ISO 10993-5:2009 guidelines [47] by the neutral red uptake (NRU) assay and MTT assay, using the mice fibroblast cell line BALB/c 3T3 clone A31 (American Type Culture Collection). Due to the observed high liquid absorption of the samples, the volume of extraction medium absorbed by each 100 mg of material was determined in accordance with ISO 10993-12:2012 protocol prior to extract

preparation. This additional volume was then added to every 100 mg in the extraction mixture during extraction of the material. The highest extract concentration tested was 50 mg/mL. The materials were UV-sterilized using UV-C light at a wavelength of 254 nm for 30 minutes, ensuring uniform exposure by gentle mixing of the powder several times during the process. The extracts were sterilized by filtration using a filter with a pore size of 0.2 µm. Extracts were prepared by incubating the samples in DMEM medium with 5% bovine serum for 24 hours at 37 ◦C with stirring. The extracts were sterilized by filtration. The cells were treated with seven dilutions of each extract in a two-dilution series for 24 hours. Highly cytotoxic latex and non-cytotoxic polyethylene film were used as reference materials. A material is considered to have cytotoxic potential when the cell viability is less than 70%. In our study, the experiments were performed in triplicate ($n \geq 3$). The data are presented as mean values ± SD.

Antimicrobial activity

The antimicrobial activity of the composites was tested against *Staphylococcus aureus* NCTC9789 and *Pseudomonas aeruginosa* PAO1161 from the IBB strain collection. This was assessed via the disk diffusion method, where bacterial suspensions of 0.5 McFarland standard were streaked in three different directions on 60 mL Mueller-Hinton agar. Then, the composites were placed on the streaked plate and co-incubated with bacteria for 24 hours at 37 °C. After the incubation time, the zone of growth inhibition was measured. Statistical analysis was performed by GraphPad Prism 10.4.2. Normality was tested using the Shapiro-Wilk test and group comparison was carried out by one-way ANOVA with Dunnett post-hoc test.

Results and Discussion

Physicochemical parameters of AgHA powder

The first step involved the synthesis of hydroxyapatite enriched with silver ions, intended to serve as a source of silver in some of the composites. Figure 1S in the Supplementary Materials presents the results of physicochemical studies for the AgHA powder and the reference material (non-substituted HA). All reflections in both PXRD patterns confirm the successful synthesis of hydroxyapatite (compared to JCPDS 09-0432) and the absence of other crystalline phases. The reflections in the AgHA diffractogram are broad and diffuse, typical for weakly crystalline materials. Crystallite size parameters calculated using the Scherrer formula along the *a* and *c* axes indicate that both materials are nanocrystalline, with crystals elongated along the *c* axis. This feature is observed in both the HA and AgHA samples (HA: 35±4 nm/16 ± 3 nm; Ag-HA: 26±4 nm/8 ±2 nm). FT-IR spectra further confirm the nanocrystalline nature of the obtained materials. The poor resolution of the ν_4 band of orthophosphates in the 650–500 cm^{-1} range in both spectra, along with a very weak band corresponding to structural hydroxyl groups at 3570 cm^{-1}, supports this conclusion. Additionally, the $\nu_1+\nu_3$ bands of orthophosphates are broad and less resolved in the spectrum of the AgHA sample, corroborating its lower crystallinity compared with the HA sample.

TEM images (Figure 1S) show small, elongated crystals of the synthesized materials, typically compacted into large agglomerates. According to the literature, incorporating silver ions into the hydroxyapatite structure reduces crystallinity, suggesting their successful into the crystal lattice [44]. The silver content in the AgHA sample, as determined by the F-AAS method, is 0.25 wt.%, which corresponds to 83% of the nominal amount introduced.

SEM microscopy

Cross-sectional SEM images of the obtained matrices are shown in Figure 1. All samples exhibit very high porosity across the entire analysed surface. The pores are interconnected and display irregular shapes and sizes, which is typical for polysaccharide materials subjected to freezing and lyophilization processes. Samples without hydroxyapatite (Figures C1Ag-n, C2Ag-n, C3Ag-n) exhibit a fibrous structure with relatively large pores ranging from 50 to 200 µm. High-magnification images reveal the presence of silver nanoparticles deposited on the surface of the fibers (marked with red arrows) [48].

Figure 1. SEM images of all obtained composites.

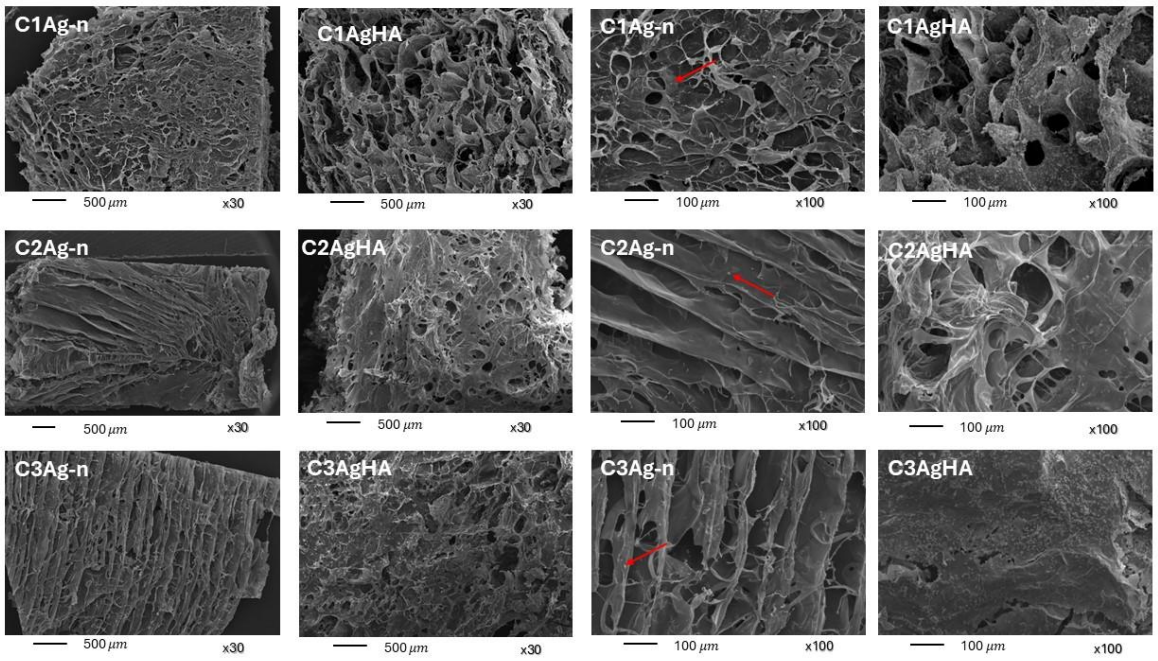

The ultrastructure of composites containing Ag-HA appears slightly more compact and dense, resembling a sponge. Hydroxyapatite is deposited on the polymer fibers and partially fills the structure, effectively reducing porosity (with pore sizes not exceeding 100 µm). Additionally, it is observed that samples with the highest chitosan-to-alginate weight ratio (C1AgHA and C1Ag-n) exhibit a relatively disordered network and irregular structure, alongside higher porosity. This may indicate the formation of more random networks during the freezing process.

ATR-FTIR analysis

The FT-IR spectra of all obtained composites and their individual components are provided in the supplementary materials (Figures 2S and 3S). Figure 2S shows the spectra of composites containing silver-doped hydroxyapatite (AgHA). By analyzing the spectra of the individual components, the presence of hydroxyapatite in all samples can be confirmed, as well as the presence of the respective polymers and ciprofloxacin. The detailed band assignments are presented below. Characteristic hydroxyapatite bands appear around 1100, 1040, 870, 610, and 560 cm^{-1}. The bands at 1100 and 1040 cm^{-1} correspond to phosphate stretching vibrations, while the band at 870 cm^{-1} is attributed to bending vibrations of carbonate groups (CO_3^{2-}) substituting phosphate groups. Bands near 610 and 560 cm^{-1} represent phosphate bending modes.

Bands observed at 2930, 1603, 1410, 1305, and 820 cm^{-1} are mainly attributed to alginate, which is the major component of the composite. The 2930 cm^{-1} band corresponds to -CH stretching, 1603 and 1410 cm^{-1} to asymmetric and symmetric stretching of -O-C-O groups and bending of -C-OH, 1305 cm^{-1} to -C-C-H and -O-C-H bending within the pyranose rings, and 820 cm^{-1} to mannuronic acid residues.

Additional bands at 2865, 1650, and 1170 cm^{-1} indicate the presence of chitosan. These correspond to -CH_2 stretching (2865 cm^{-1}), amide -C=O stretching (1650 cm^{-1}), and -C-O-C stretching vibrations (1170 cm^{-1}).

Moreover, characteristic bands of ciprofloxacin are visible at 1270 and 805 cm^{-1}, associated with -C-F stretching and aromatic ring vibrations, respectively, confirming its presence in the composites.

Analysis of the FT-IR spectra of composite samples containing silver nanoparticles (Figure 3S) reveals the presence of intense, broad bands in the 1170–940 cm^{-1} region, which result from overlapping signals characteristic of alginate and chitosan.

As shown by comparison with literature data for the characteristic bands of the individual components [49–54], not all expected bands are visible in the recorded spectra. This is because some bands appear within the same wavenumber range; therefore, more intense bands may overshadow those with lower intensity. Nevertheless, the spectral analysis confirms that the obtained composites are composed as intended, comprising an organic phase of natural polymers, an inorganic hydroxyapatite phase, and the antibiotic ciprofloxacin.

Swelling behaviour

A parameter closely associated with the porosity and ultrastructure of biomaterials is the swelling coefficient. In this study, the swelling behaviour was evaluated at pH 7.4 and a temperature of 37 °C to closely mimic the physiological conditions of the bone tissue environment. Notably, porous matrices with swelling capability are highly effective for both bone tissue regeneration and reconstruction. This is due to their ability to facilitate fluid flow within swollen pores, ensuring nutrient mass transfer to cells while aiding in the removal of metabolic waste. Furthermore, swelling biomaterials can serve as carriers for drug substances and other biologically active compounds, primarily due to enhanced diffusion properties [55].

Figure 2 presents the swelling results for all tested materials over a 48-hour period. The samples exhibited variability in both the degree of swelling and the rate at which this process occurred. Materials with higher chitosan-to-alginate ratios demonstrated lower swelling capacities (absorption of aqueous solution), which can be attributed to the reduced hydrophilicity of chitosan compared to alginate. Additionally, the findings reveal that the incorporation of hydroxyapatite in the composites significantly reduces their swelling capacity [56].

Consequently, the sample with the lowest swelling coefficient was C1AgHA (approximately 382%), whereas the highest swelling capacity was observed for C2Ag-n (1170%).

Figure 2. Swelling test. The graph shows the swelling ratio (%) of the obtained materials at different times.

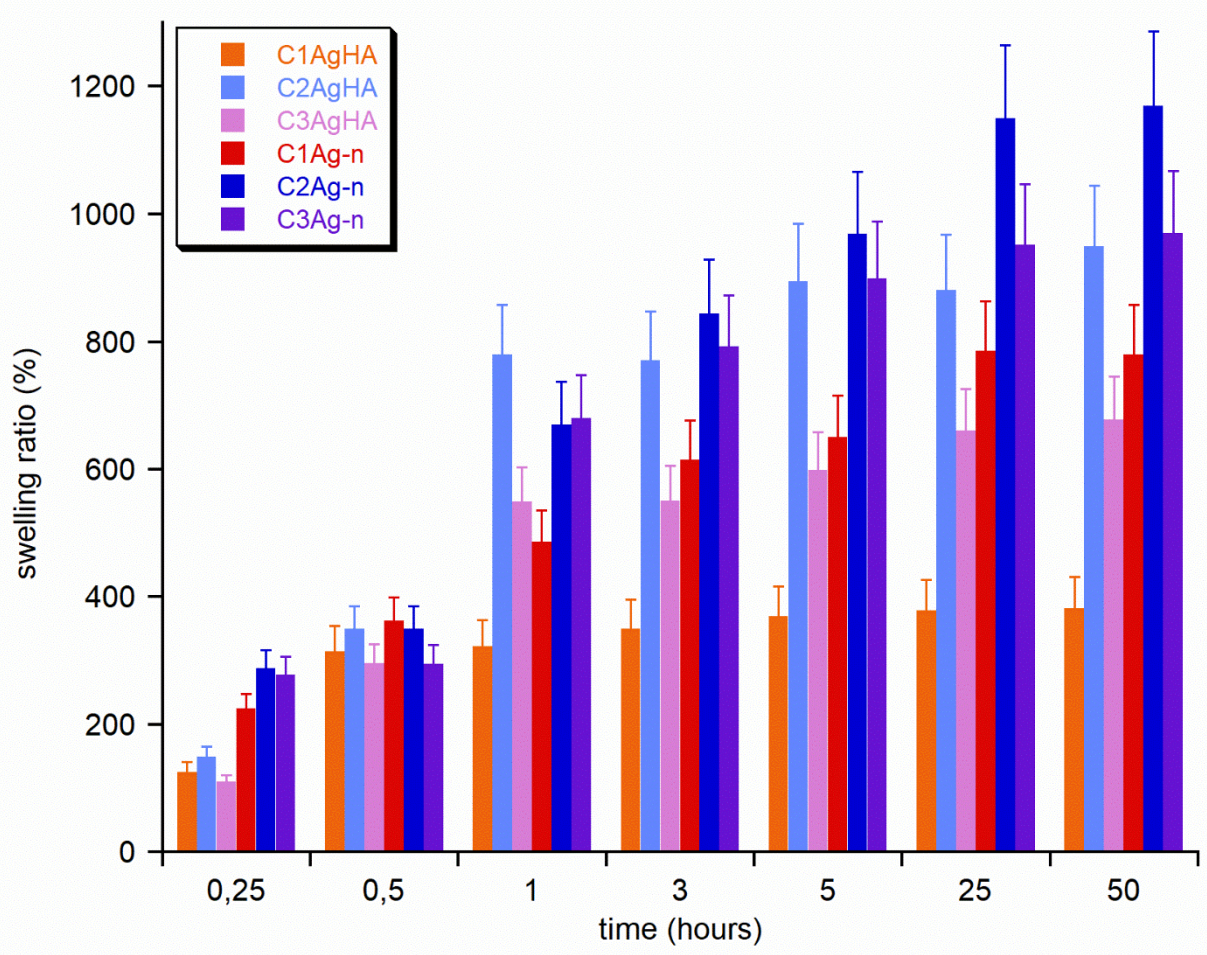

Antibiotic release

The ciprofloxacin loading efficiency was determined to be 95.2±1.1% across the tested composite. The evaluation of drug loading efficiency was made possible by quantifying the loss of ciprofloxacin during the cross-linking and rinsing processes of the composite suspensions. This loss corresponded to 4.8±1.1% relative to the total amount of drug introduced per composite, i.e. 100 mg of ciprofloxacin per 1 g of the composite. The HPLC chromatograms

(Figure 4S in Supplementary Materials) of the drug substance after 28 days confirmed the chemical stability of ciprofloxacin, showing consistent retention times and peak shapes comparable to the reference standard, with no evidence of degradation products.

The ciprofloxacin release profiles from each matrix are depicted in Figures 3a and 3b. All curves exhibit relatively similar release patterns, differing primarily in the quantity of drug released. Hydroxyapatite demonstrates the most pronounced effect on ciprofloxacin release, as its presence in the material significantly attenuates drug release. This effect may be attributed to the adsorption of ciprofloxacin molecules onto hydroxyapatite crystals through intermolecular interactions, such as van der Waals forces or the reduction in porosity within hydroxyapatite-containing materials [57,58].

Figure 3. Ciprofloxacin release profiles from the composite matrices: full release curves over 672 hours (a), initial release phase - first 48 hours (b); representative model fittings to Korsmeyer-Peppas model for C3AgHA in the short- and long-term release ranges (c, d – respectively).

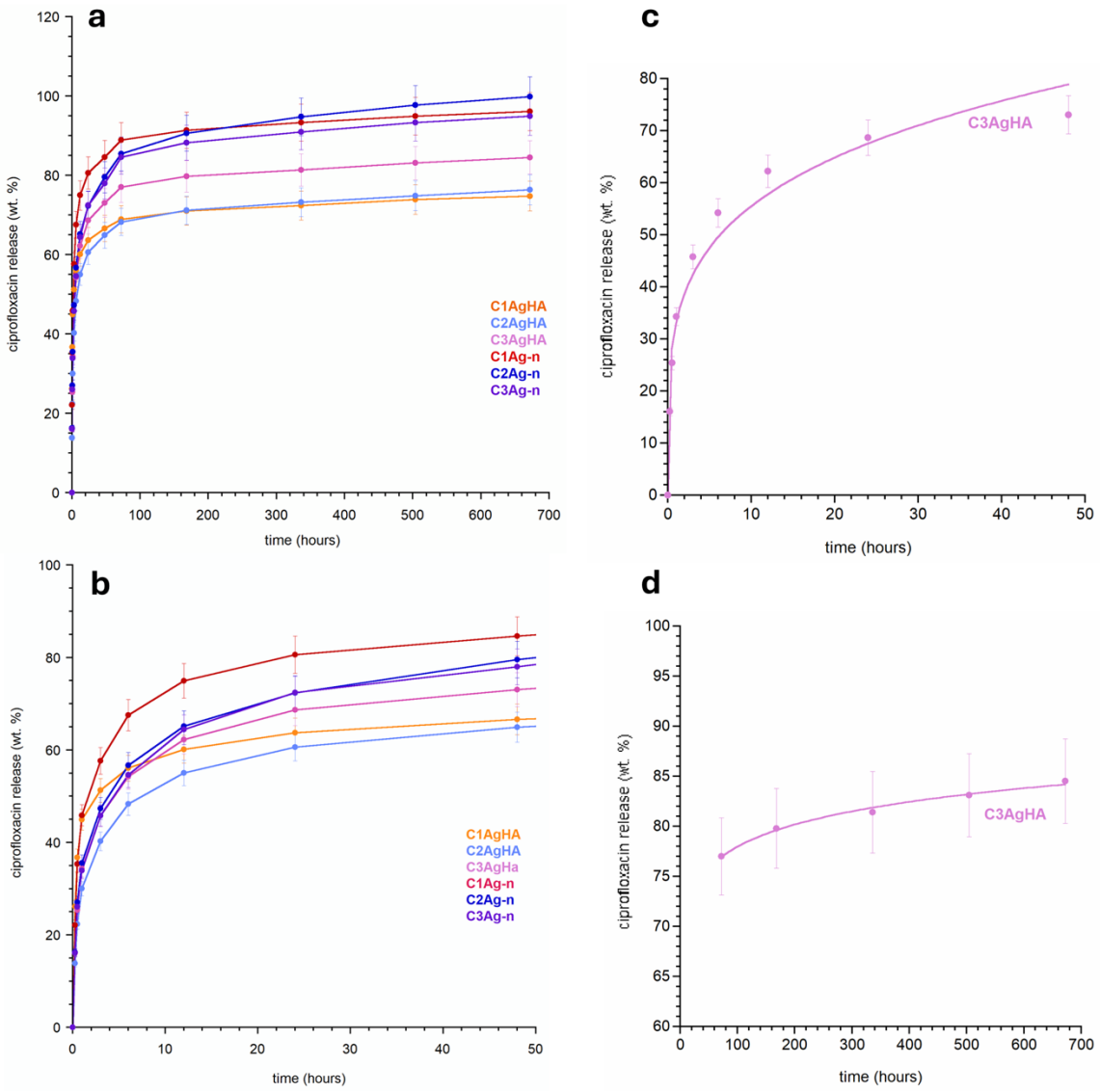

The experimental data were fitted to various mathematical models of drug release, including the zero-order, first-order, Higuchi, Korsmeyer-Peppas (K-P), Weibull, and Peppas-Sahlin models [59–61]. The Peppas–Sahlin and Weibull models were preliminarily tested using one representative release profile. However, the obtained fitting parameters and curve shapes were inconsistent with the experimental data and the biphasic character of the release process. Therefore, these models were not further applied to all samples and were excluded from the main analysis.

Representative fitting parameters and R^2 coefficients for selected ciprofloxacin release models for one sample are presented in Table 1S in the Supplementary Materials.

A detailed analysis indicated that the K-P model provided the best fit, dividing the release into two phases: an initial phase up to 48 hours and a subsequent phase spanning 48 to 672 hours. The K-P model is frequently used to characterize the release of active substances from carriers such as hydrogels, polymer films, and biomaterial composites [60]. The fitting data, presented in Table 2, reveal that in the first phase, the release mechanism is predominantly diffusion-driven but atypically slow compared to standard Fickian diffusion ($n<0.45$). The second phase is characterized by an even lower n value ($n \ll 0.45$, specifically $n=0.035-0.070$), suggesting extremely slow diffusion. When n approaches zero, the release approximates zero-order kinetics, maintaining a nearly constant rate over time.

In these matrices, the observed slowing of release may result from the depletion of ciprofloxacin in readily accessible regions, leading to a significant reduction in the concentration gradient. The increased k_{KP} value during this phase (nearly doubling for each sample) suggests the involvement of additional release mechanisms, potentially linked to matrix relaxation and polysaccharide swelling, particularly alginate [58,61,62]. These complex mechanisms warrant further investigation.

Table 2. Summary of fitting parameters for ciprofloxacin and silver release.

	Ciprofloxacin release							
Sample	I phase (0-48 hours)				II phase (48-672 hours)			
	k_{KP}	n	R^2	Model	k_{KP}	n	R^2	model
C1AgHA	8.7±0.4	0.14±0.01	0.9840	K-P	12.5±0.1	0.036±0.001	0.9955	K-P
C2AgHA	7.1±0.5	0.23±0.02	0.9831	K-P	13.4±0.1	0.048±0.002	0.9975	K-P
C3AgHA	9.4±0.6	0.22±0.02	0.9833	K-P	18.3±0.2	0.040±0.002	0.9947	K-P
C1Ag-n	15.0±0.9	0.19±0.02	0.9799	K-P	26.5±0.2	0.035±0.001	0.9980	K-P
C2Ag-n	15.4±0.9	0.23±0.02	0.9868	K-P	28.5±0.2	0.070±0.001	0.9996	K-P
C3Ag-n	13.6±0.8	0.23±0.02	0.9877	K-P	27.9±0.3	0.051±0.002	0.9982	K-P
	Ag release							
	I phase (0-48 hours)				II phase (48-672 hours)			
C1AgHA	6.0±0.4	0.17±0.02	0.9604	K-P	8.8±0.3	0.058±0.005	0.9885	K-P
C2AgHA	1.04±0.04	0.23±0.02	0.9905	K-P	1.6±0.2	0.14±0.02	0.9627	K-P
C3AgHA	2.2±0.1	0.27±0.02	0.9850	K-P	4.1±0.2	0.107±0.007	0.9944	K-P
					Q_0	k	R^2	
C1Ag-n	1.06±0.04	0.24±0.01	0.9921	K-P	2.16±0.06	0.012±0.001	0.9998	Zero order
C2Ag-n	3.3±0.2	0.21±0.03	0.9671	K-P	7.2±0.2	0.0029±0.0004	0.9682	Zero order
C3Ag-n	1.64±0.08	0.28±0.02	0.9937	K-P	4.8±0.20	0.0154±0.0005	0.9984	Zero order

Silver Release

Similar to ciprofloxacin, the loading efficiency of silver nanoparticles and the silver content incorporated into HA within the composites were also determined. In contrast to ciprofloxacin, significant losses of silver occurred during the cross-linking and rinsing of the composite suspensions. The loading efficiency of silver nanoparticles was 29.3±2.6% whereas the efficiency of silver incorporation in HA-containing composites amounted to 20.4±1.3%. The experimental curves depicting silver release from the composites are analyzed in a similar manner. Figure 4a presents the experimental release profiles for all matrices, while Figures 4b-c and 4d-e detail the fits for samples containing hydroxyapatite enriched with silver ions or silver nanoparticles, respectively. Representative fitting parameters and R^2 coefficients for selected Ag^+ release models for two samples are presented in Table 2S in the Supplementary Materials.

Figure 4. Silver release profiles from all composite matrices (a), model fitting results for materials with silver-ion-doped hydroxyapatite (b–c), fitted release curves for composites containing hydroxyapatite with embedded silver nanoparticles (d–e).

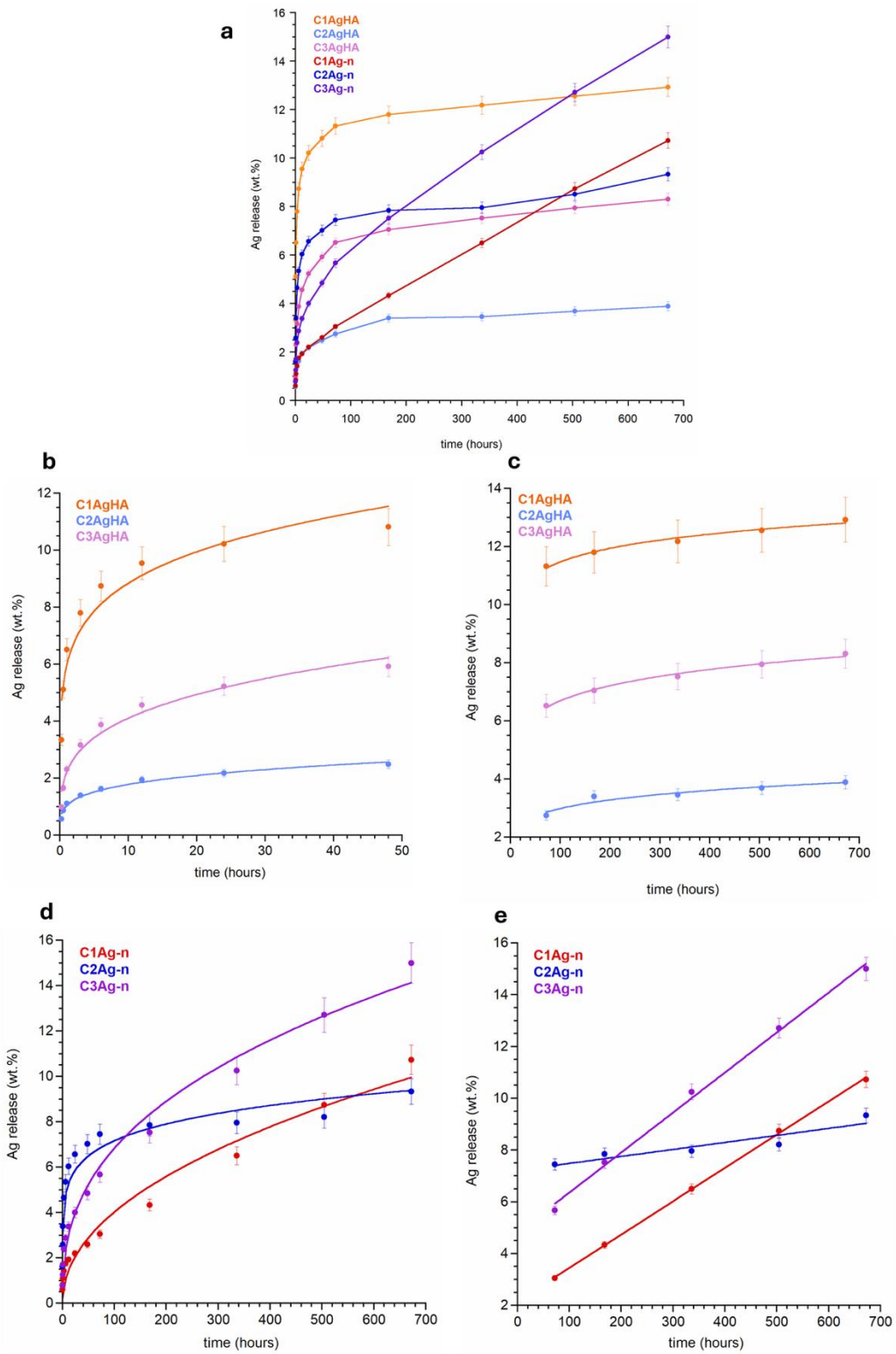

In contrast to ciprofloxacin release, which reaches 75–99% within 28 days (depending on the sample), the silver release profiles indicate markedly slower release rates, ranging from 4% to 15%. Previous studies on ion release (e.g., selenium, zinc, silver, and gallium) from nanocrystalline hydroxyapatite and various composite matrices have similarly demonstrated slow release over comparable timeframes (4–5 weeks) relative to drug substances [20,44,63]. This may result from strong interactions between ions/nanoparticles and the matrix components, particularly alginate and/or chitosan. For example, silver ions may bind to negatively charged groups within the alginate matrix, while in chitosan matrices, complexes may form between silver ions and amine groups [64]. Such binding can impede ion release, causing significant delays.

Figures 4b and 4c suggest that silver ions exhibit stronger binding to alginate than to chitosan. A similar trend is observed for silver nanoparticles (Figures 4d and 4e). The fitting parameters for silver release are summarized in Table 2. The data suggest that, similar to ciprofloxacin, the silver release process can be divided into two distinct phases, with a transition point at 48 hours.

During the first phase, all curves fit well to the K-P model, with n-values ranging from 0.17 to 0.28, indicating Fickian diffusion. In the second phase (48–672 hours), the release of silver ions from hydroxyapatite-containing matrices is also best described by the Korsmeyer-Peppas model. However, as with ciprofloxacin, the diffusion process is significantly restricted ($n=0.058-0.14$).

For samples C1Ag-n, C2Ag-n, and C3Ag-n (containing nanoparticles), the release data in the second phase can be accurately described ($R^2=0.9682-0.9998$) using the zero-order kinetics model [59,65]. In this phase, silver ion release occurs at a constant rate, independent of concentration. The zero-order release observed in the second phase may be associated with matrix swelling, relaxation, and reduced nanoparticle-matrix interactions [61].

The biphasic release profiles observed for ciprofloxacin and silver species can be correlated with the hydration behaviour of the matrices. Rapid water uptake during the initial hours promoted the swelling of the polysaccharide network, increasing the diffusion pathways for drug molecules. As the system reached equilibrium hydration, the matrix structure became denser due to partial gelation and polymer rearrangement, which limited further diffusion and resulted in a slower release rate.

Cytotoxicity Assay

Table 3 shows the results of the MTT and NRU test for the highest tested concentration for the silver-doped hydroxyapatite (AgHA) and silver nanoparticle (Ag-N) composites. According to the NRU and MTT test methodologies, none of the seven tested dilutions of either material extract was classified as cytotoxic, since no decrease in cell viability was observed in either of the two cytotoxicity assessment tests (Table 3S and 4S). These results indicate that both silver-doped hydroxyapatite composites (AgHA) and silver nanoparticles (Ag-N) composites are biocompatible with the normal cells used in the tests, suggesting that the applied production process and concentrations maintain cell viability and do not cause cytotoxic effects. Similar findings were reported by Sinulingga et al. [66], who showed that silver and magnesium or zinc co-doped hydroxyapatite did not significantly reduce the viability of MC3T3-E1 cells in MTT assay performed according to ISO 10993-5, while providing strong antibacterial properties. On the other hand, slight cytotoxicity was observed in a publication from our team [67], where silver ion-doped hydroxyapatite granules showed reduced cell viability at higher concentrations in standard cell lines, indicating some cytotoxic potential. Additionally, Afhkami et al. [68] reported slight decreases in MC3T3-E1 preosteoblast viability after exposure to silver nanoparticles. These different outcomes show that the biocompatibility of silver-containing biomaterials depends on factors such as the concentration of silver, the form of the nanoparticles and the production methods used.

Table 3. MTT and NRU test results for the highest concentrations of test extracts (50 mg/mL) compared to the untreated control.

Sample	MTT test - cells viability ± SD (%)	NRU test - cells viability ± SD (%)	Classification
C1AgHA	114 ± 1	109 ± 5	Non-cytotoxic
C1Ag-n	118 ± 13	106 ± 15	Non-cytotoxic
C2AgHA	111 ± 4	94 ± 7	Non-cytotoxic
C2Ag-n	115 ± 4	102 ± 8	Non-cytotoxic
C3AgHA	139 ± 4	113 ± 5	Non-cytotoxic
C3Ag-n	121 ± 15	94 ± 13	Non-cytotoxic
LT	2 ± 3	3 ± 2	Cytotoxic
PE	113 ± 3	99 ± 1	Non-cytotoxic

LT—latex, reference cytotoxic material. PE—polyethylene film, reference non-cytotoxic material. SD—standard deviation. A decrease in the cell viability below 70% classifies the sample as cytotoxic.

Microbiology

The disc diffusion method was used to assess the antimicrobial activity of composites enriched with silver ions against the multi-drug-resistant bacterial strain *S. aureus* NCTC9789 and *P. aeruginosa* PAO1161. The zone of growth inhibition was measured and compared between the composites and controls. All of the composites exhibited significant antimicrobial activity against both pathogenic strains (Table 4). The largest zone of inhibition for *S. aureus* NCTC9789 was observed for the composites C2AgHA, C3Ag-n and C1Ag-n, respectively, however, the zone of inhibition for all composites ranged from 2.6-3.2 cm. In turn, for *P. aeruginosa* PAO1161, a higher antimicrobial activity of the composites was observed, measuring 3.3-3.7 cm of the zone of growth inhibition. The highest inhibition of growth for this pathogen was shown for the composites C3AgHA, C1AgHA and C2AgHA.

Table 4. Zone of growth inhibition for pathogenic strains. Results are shown as mean ± SD (n=3). The values for the zone of growth inhibition are presented in cm. C1 and C3 are control composites, lacking antibiotics and silver ions (chitosan and alginate matrices). The statistical difference between control and treatment is presented by **** p<0.0001.

Composite/strain	*S. aureus* NCTC9789	*P. aeruginosa* PAO1161
C1Ag-n	3.0 ± 0.2 ****	3.3 ± 0.3 ****
C2AgHA	3.2 ± 0.2 ****	3.6 ± 0.2 ****
C1AgHA	2.9 ± 0.4 ****	3.7 ± 0.2 ****
C3Ag-n	3.2 ± 0.2 ****	3.5 ± 0.3 ****
C2Ag-n	2.8 ± 0.2 ****	3.5 ± 0.1 ****
C1	0 ± 0	0 ± 0
C3AgHA	2.6 ± 0.1 ****	3.7 ± 0.1 ****
C3	0 ± 0	0 ± 0

In the literature, several studies have reported microbiological results for materials containing silver or ciprofloxacin, demonstrating their well-established antibacterial potential. When it comes to silver nanoparticles, 11.2 to 18.8 mm inhibition zone was shown against *E. coli* with the increase of Ag-NPs content (%) in the composite films [69]. Nano-silver loaded poly(styrene-co-acrylic) (nAg-PSA) composites had maximum diameters of inhibition zones against the *E. coli* (1.18 mm) and *S. aureus* (1.29 mm) [70] and other studies confirm an inhibition zone of nanoparticles up to around 20 mm [71].

For ciproflaxin-loaded composites, e.g. ciprofloxacin-loaded polymeric fiber mats containing 0.25%, 0.5%, and 1% ciprofloxacin showed inhibition zones against *E. Coli* (≈28 mm) and *S. aureus* (≈20 mm) [72], other studies showing up to 37 mm inhibition [73].

P. aeruginosa and *S. aureus* have a strong natural resistance to many antibiotics, which limits treatment options. Therefore, silver nanoparticles (AgNPs) are being investigated as promising alternatives for preventing and controlling infections [5,6]. Our results show enhanced antimicrobial activity of ciprofloxacin as to what is commonly found in other studies testing the mere antibiotic activity for these strains (around 25-33mm) [74,75]. Our results also show greater antibiotic susceptibility of Gram-negative *P. aueruginosa*, which can be attributed to the thinner peptidoglycan layer as opposed to Gram-positive *S. aureus*, which with a thicker peptidoglycan layer functioning as a barrier against nanoparticles. Moreover, silver ions more easily bind to negatively charged surfaces, such as lipopolysaccharides found in the outer membrane of Gram-negative bacteria. This observation can be explained by the synergistic effect between silver nanoparticles and ciprofloxacin. While ciprofloxacin efficiently penetrates the outer membrane of Gram-negative bacteria, silver nanoparticles can further increase membrane permeability and induce oxidative stress, leading to enhanced bactericidal activity against *P. aeruginosa* compared to *S. aureus*. The differences in antibacterial activity among the composite materials may result from the composition of their matrices; those containing a higher amount of chitosan exhibit slightly increased antibacterial activity, which is consistent with the known properties of chitosan. In the future, it would be valuable to investigate the antimicrobial activity of the solutions after a prolonged period of silver ion release, once the antibiotic has been completely released from the composite. At that point, the composites containing silver ions could potentially retain antimicrobial activity, this time due to the action of the silver ions themselves. As shown in Figure 4, the release of silver ions increases over time, suggesting that such a study could yield highly interesting results. This will be the focus of our upcoming research.

Conclusions

In this study, novel polysaccharide-based composite materials were successfully developed using chitosan and alginate matrices reinforced with sericin and loaded with ciprofloxacin and silver, the latter introduced either as ions within nanocrystalline hydroxyapatite or as silver nanoparticles. The combination of the solid–liquid method with lyophilization enabled the formation of highly porous structures, as confirmed by SEM observations. The composites demonstrated sustained release of both ciprofloxacin and silver species for up to 28 days. Mathematical modeling of the release kinetics revealed a biphasic mechanism for ciprofloxacin and silver ions, initially governed by diffusion through the swollen matrix and subsequently by matrix relaxation and gelation processes. In contrast, silver nanoparticles displayed an increased release in the second phase, following zero-order kinetics.

All silver-containing materials showed pronounced antibacterial activity against *Staphylococcus aureus* (NCTC 9789) and *Pseudomonas aeruginosa* (PAO1161), including multi-drug resistant strains. These results confirm the dual functionality of the composites, which can act simultaneously as temporary bone fillers and localized drug delivery systems, capable of supporting bone tissue regeneration while preventing infection associated with orthopedic implants.

The present findings emphasize the added value of combining polysaccharide matrices with sericin reinforcement and dual antimicrobial agents. Such an approach allows for tunable release profiles and prolonged antimicrobial protection, addressing one of the major clinical challenges in orthopedic and reconstructive surgery—post-implant infections in poorly vascularized tissues.

However, this study has several limitations. Our research aimed to evaluate the synergistic effect of the dual-loaded (silver and ciprofloxacin) composites, rather than to quantify the

independent contribution of each component. We plan to continue the studies focusing on quantifying the synergistic effect between ciprofloxacin and silver nanoparticles. The biological assays were limited to *in vitro* antibacterial evaluation and the mechanical and degradation behavior under physiological conditions was not investigated.

Future research should therefore focus on detailed mechanical testing and *in vivo* evaluation to validate the biological safety and therapeutic performance of the developed composites. Expanding this concept towards multifunctional scaffolds with enhanced osteoinductive and angiogenic properties could further advance their application in bone tissue engineering and localized infection control using such materials as local dressings for bone wounds.

References

[1] E. Kasapgil, M. Garay-Sarmiento, C. Rodriguez-Emmenegger, Advanced Antibacterial Strategies for Combatting Biomaterial-Associated Infections: A Comprehensive Review, WIREs Nanomedicine Nanobiotechnology 16 (2024) e2018. https://doi.org/10.1002/wnan.2018.

[2] N. Blanco-Cabra, J. Alcàcer-Almansa, J. Admella, B.V. Arévalo-Jaimes, E. Torrents, Nanomedicine against biofilm infections: A roadmap of challenges and limitations, WIREs Nanomedicine Nanobiotechnology 16 (2024) e1944. https://doi.org/10.1002/wnan.1944.

[3] N.A. Hodges, E.M. Sussman, J.P. Stegemann, Aseptic and septic prosthetic joint loosening: Impact of biomaterial wear on immune cell function, inflammation, and infection, Biomaterials 278 (2021) 121127.

[4] E. Tacconelli, E. Carrara, A. Savoldi, S. Harbarth, M. Mendelson, D.L. Monnet, C. Pulcini, G. Kahlmeter, J. Kluytmans, Y. Carmeli, Discovery, research, and development of new antibiotics: the WHO priority list of antibiotic-resistant bacteria and tuberculosis, Lancet Infect. Dis. 18 (2018) 318–327.

[5] S. Tang, J. Zheng, Antibacterial Activity of Silver Nanoparticles: Structural Effects, Adv. Healthc. Mater. 7 (2018) 1701503. https://doi.org/10.1002/adhm.201701503.

[6] B. Le Ouay, F. Stellacci, Antibacterial activity of silver nanoparticles: A surface science insight, Nano Today 10 (2015) 339–354.

[7] W.K. Jung, H.C. Koo, K.W. Kim, S. Shin, S.H. Kim, Y.H. Park, Antibacterial Activity and Mechanism of Action of the Silver Ion in *Staphylococcus aureus* and *Escherichia coli*, Appl. Environ. Microbiol. 74 (2008) 2171–2178. https://doi.org/10.1128/AEM.02001-07.

[8] K. Mijnendonckx, N. Leys, J. Mahillon, S. Silver, R. Van Houdt, Antimicrobial silver: uses, toxicity and potential for resistance, BioMetals 26 (2013) 609–621. https://doi.org/10.1007/s10534-013-9645-z.

[9] Q.L. Feng, J. Wu, G.Q. Chen, F.Z. Cui, T.N. Kim, J.O. Kim, A mechanistic study of the antibacterial effect of silver ions onEscherichia coli andStaphylococcus aureus, J. Biomed. Mater. Res. 52 (2000) 662–668. https://doi.org/10.1002/1097-4636(20001215)52:4<662::AID-JBM10>3.0.CO;2-3.

[10] X. Guo, P. Song, F. Li, Q. Yan, Y. Bai, J. He, Q. Che, H. Cao, J. Guo, Z. Su, Research Progress of Design Drugs and Composite Biomaterials in Bone Tissue Engineering, Int. J. Nanomedicine Volume 18 (2023) 3595–3622. https://doi.org/10.2147/IJN.S415666.

[11] S. Mondal, U. Pal, 3D hydroxyapatite scaffold for bone regeneration and local drug delivery applications, J. Drug Deliv. Sci. Technol. 53 (2019) 101131.

[12] V. Mouriño, J.P. Cattalini, J.A. Roether, P. Dubey, I. Roy, A.R. Boccaccini, Composite polymer-bioceramic scaffolds with drug delivery capability for bone tissue engineering, Expert Opin. Drug Deliv. 10 (2013) 1353–1365. https://doi.org/10.1517/17425247.2013.808183.

[13] J. Venkatesan, I. Bhatnagar, P. Manivasagan, K.-H. Kang, S.-K. Kim, Alginate composites for bone tissue engineering: A review, Int. J. Biol. Macromol. 72 (2015) 269–281.

[14] N. Farshidfar, S. Iravani, R.S. Varma, Alginate-based biomaterials in tissue engineering and regenerative medicine, Mar. Drugs 21 (2023) 189.

[15] J. Fourie, F. Taute, L. Du Preez, D. De Beer, Chitosan Composite Biomaterials for Bone Tissue Engineering—a Review, Regen. Eng. Transl. Med. 8 (2022) 1–21. https://doi.org/10.1007/s40883-020-00187-7.

[16] H. Li, F. Jiang, S. Ye, Y. Wu, K. Zhu, D. Wang, Bioactive apatite incorporated alginate microspheres with sustained drug-delivery for bone regeneration application, Mater. Sci. Eng. C 62 (2016) 779–786.

[17] Y. Bi, Z. Lin, S. Deng, Fabrication and characterization of hydroxyapatite/sodium alginate/chitosan composite microspheres for drug delivery and bone tissue engineering, Mater. Sci. Eng. C 100 (2019) 576–583.

[18] Y. Song, Q. Hu, Q. Liu, S. Liu, Y. Wang, H. Zhang, Design and fabrication of drug-loaded alginate/hydroxyapatite/collagen composite scaffolds for repairing infected bone defects, J. Mater. Sci. 58 (2023) 911–926. https://doi.org/10.1007/s10853-022-08053-3.

[19] F. Ordikhani, A. Simchi, Long-term antibiotic delivery by chitosan-based composite coatings with bone regenerative potential, Appl. Surf. Sci. 317 (2014) 56–66.

[20] B. Kołodziejska, R. Figat, J. Kolmas, Biomimetic apatite/natural polymer composite granules as multifunctional dental tissue regenerative material, Int. J. Mol. Sci. 24 (2023) 16751.

[21] I. Arzate-Vázquez, J.J. Chanona-Pérez, G. Calderón-Domínguez, E. Terres-Rojas, V. Garibay-Febles, A. Martínez-Rivas, G.F. Gutiérrez-López, Microstructural characterization of chitosan and alginate films by microscopy techniques and texture image analysis, Carbohydr. Polym. 87 (2012) 289–299.

[22] A.R. Costa-Pinto, R.L. Reis, N.M. Neves, Scaffolds Based Bone Tissue Engineering: The Role of Chitosan, Tissue Eng. Part B Rev. 17 (2011) 331–347. https://doi.org/10.1089/ten.teb.2010.0704.

[23] T.W. Wong, W.H.N.S. Ashikin, C.L. Law, Evaporation and Diffusion Transport Properties and Mechanical Properties of Alginate Dried Film, Dry. Technol. 32 (2014) 117–125. https://doi.org/10.1080/07373937.2013.821479.

[24] K. Baysal, A.Z. Aroguz, Z. Adiguzel, B.M. Baysal, Chitosan/alginate crosslinked hydrogels: Preparation, characterization and application for cell growth purposes, Int. J. Biol. Macromol. 59 (2013) 342–348.

[25] P. Dey, Bone mineralisation, in: Contemp. Top. Phosphorus Biol. Mater., IntechOpen, 2020. https://books.google.com/books?hl=en&lr=&id=TJYtEAAAQBAJ&oi=fnd&pg=PA35&dq=hydroxyapatite+mineralised+tissues&ots=xiKdNlVF5p&sig=kJdvwK43bJmLO0kDKimj9DhJ2SE (accessed May 31, 2025).

[26] R.Z. LeGeros, J.P. LeGeros, Hydroxyapatite, in: Bioceram. Their Clin. Appl., Elsevier, 2008: pp. 367–394. https://www.sciencedirect.com/science/article/pii/B9781845692049500168 (accessed May 31, 2025).

[27] T. Kono, T. Sakae, H. Nakada, T. Kaneda, H. Okada, Confusion between carbonate apatite and biological apatite (carbonated hydroxyapatite) in bone and teeth, Minerals 12 (2022) 170.

[28] J. Wang, L.L. Shaw, Nanocrystalline hydroxyapatite with simultaneous enhancements in hardness and toughness, Biomaterials 30 (2009) 6565–6572.

[29] M.U. Munir, S. Salman, I. Javed, S.N.A. Bukhari, N. Ahmad, N.A. Shad, F. Aziz, Nano-hydroxyapatite as a delivery system: overview and advancements, Artif. Cells Nanomedicine Biotechnol. 49 (2021) 717–727. https://doi.org/10.1080/21691401.2021.2016785.

[30] Y. Li, T. Wu, G. Zhang, A. Fang, Y. Li, S. Wang, H. Yan, P. Liang, J. Lian, Y. Zhang, A native sericin wound dressing spun directly from silkworms enhances wound healing, Colloids Surf. B Biointerfaces 225 (2023) 113228.

[31] S. Baptista-Silva, S. Borges, A.R. Costa-Pinto, R. Costa, M. Amorim, J.R. Dias, Ó. Ramos, P. Alves, P.L. Granja, R. Soares, M. Pintado, A.L. Oliveira, *In Situ* Forming Silk Sericin-Based Hydrogel: A Novel Wound Healing Biomaterial, ACS Biomater. Sci. Eng. 7 (2021) 1573–1586. https://doi.org/10.1021/acsbiomaterials.0c01745.

[32] J. Liu, L. Shi, Y. Deng, M. Zou, B. Cai, Y. Song, Z. Wang, L. Wang, Silk sericin-based materials for biomedical applications, Biomaterials (2022) 121638.

[33] R.I. Kunz, R.M.C. Brancalhão, L.D.F.C. Ribeiro, M.R.M. Natali, Silkworm Sericin: Properties and Biomedical Applications, BioMed Res. Int. 2016 (2016) 1–19. https://doi.org/10.1155/2016/8175701.

[34] P. Aramwit, S. Napavichayanum, P. Pienpinijtham, Y. Rasmi, N. Bang, Antibiofilm activity and cytotoxicity of silk sericin against *Streptococcus mutans* bacteria in biofilm: an *in vitro* study, J. Wound Care 29 (2020) S25–S35. https://doi.org/10.12968/jowc.2020.29.Sup4.S25.

[35] P. Ghensi, E. Bettio, D. Maniglio, E. Bonomi, F. Piccoli, S. Gross, P. Caciagli, N. Segata, G. Nollo, F. Tessarolo, Dental implants with anti-biofilm properties: a pilot study for developing a new sericin-based coating, Materials 12 (2019) 2429.

[36] G.T. Hailu, M.T. Alemea, F. Lemessa, Development of silk sericin-based polysaccharide-protein hybrid biofilms: Mechanical, thermal, and antibacterial properties, Res. 2 (2025) 100097.

[37] S. Sunarintyas, W. Siswomihardjo, The effect of sericin application over hydroxyapatite surface on osteoblast cells proliferation, in: 2011 2nd Int. Conf. Instrum. Commun. Inf. Technol. Biomed. Eng., IEEE, 2011: pp. 145–149. https://ieeexplore.ieee.org/abstract/document/6108613/ (accessed May 31, 2025).

[38] C. Noosak, P. Jantorn, J. Meesane, S. Voravuthikunchai, D. Saeloh, Dual-functional bioactive silk sericin for osteoblast responses and osteomyelitis treatment, PLoS One 17 (2022) e0264795.

[39] S. Nayak, T. Dey, D. Naskar, S.C. Kundu, The promotion of osseointegration of titanium surfaces by coating with silk protein sericin, Biomaterials 34 (2013) 2855–2864.

[40] M. Jiang, S. Li, P. Ming, Y. Guo, L. Yuan, X. Jiang, Y. Liu, J. Chen, D. Xia, Y. He, G. Tao, Rational design of porous structure-based sodium alginate/chitosan sponges loaded with green synthesized hybrid antibacterial agents for infected wound healing, Int. J. Biol. Macromol. 237 (2023) 123944. https://doi.org/10.1016/j.ijbiomac.2023.123944.

[41] A. Kyzioł, A. Mazgała, J. Michna, A. Regiel-Futyra, V. Sebastian, Preparation and characterization of alginate/chitosan formulations for ciprofloxacin-controlled delivery, J. Biomater. Appl. 32 (2017) 162–174. https://doi.org/10.1177/0885328217714352.

[42] Q. Ma, S. Salathia, M.R. Gigliobianco, C. Casadidio, P. Di Martino, R. Censi, Recent Insights into the Potential and Challenges of Sericin as a Drug Delivery Platform for Multiple Biomedical Applications, Pharmaceutics 17 (2025) 695. https://doi.org/10.3390/pharmaceutics17060695.

[43] C. Noosak, K. Iamthanaporn, J. Meesane, S.P. Voravuthikunchai, D.S. Sotthibandhu, Bioactive functional sericin/polyvinyl alcohol hydrogel: biomaterials for supporting orthopedic surgery in osteomyelitis, J. Mater. Sci. 58 (2023) 5477–5488. https://doi.org/10.1007/s10853-023-08356-z.

[44] K. Pajor, Ł. Pajchel, A. Zgadzaj, U. Piotrowska, J. Kolmas, Modifications of hydroxyapatite by gallium and silver ions—physicochemical characterization, cytotoxicity and antibacterial evaluation, Int. J. Mol. Sci. 21 (2020) 5006.

[45] A. Luanda, M. Mahadev, R.N. Charyulu, V. Badalamoole, Evaluation of Dual Drug Delivery Efficiency of Nanocomposite Hydrogel Containing Pectin for Combating Cancer, Polym. Adv. Technol. 36 (2025) e70118. https://doi.org/10.1002/pat.70118.

[46] C. Corsaro, G. Neri, A.M. Mezzasalma, E. Fazio, Weibull Modeling of Controlled Drug Release from Ag-PMA Nanosystems, Polymers 13 (2021) 2897. https://doi.org/10.3390/polym13172897.

[47] B. Iso, B. STANDARD, Biological evaluation of medical devices, Part 1 (2009) 10993.

[48] A. Luanda, M. Mahadev, R.N. Charyulu, V. Badalamoole, Locust bean gum-based silver nanocomposite hydrogel as a drug delivery system and an antibacterial agent, Int. J. Biol. Macromol. 282 (2024) 137097. https://doi.org/10.1016/j.ijbiomac.2024.137097.

[49] R. Varma, S. Vasudevan, Extraction, Characterization, and Antimicrobial Activity of Chitosan from Horse Mussel *Modiolus modiolus*, ACS Omega 5 (2020) 20224–20230. https://doi.org/10.1021/acsomega.0c01903.

[50] Z.Z. Zam, F. Muin, A. Fataruba, Identification of chitosan beads from coconut crab patani variety using Fourier Transform Infrared Spectroscopy (FTIR), in: J. Phys. Conf. Ser., IOP Publishing, 2021: p. 012014. https://iopscience.iop.org/article/10.1088/1742-6596/1832/1/012014/meta (accessed July 29, 2025).

[51] D. Leal, B. Matsuhiro, M. Rossi, F. Caruso, FT-IR spectra of alginic acid block fractions in three species of brown seaweeds, Carbohydr. Res. 343 (2008) 308–316.

[52] Z. Belattmania, S. Kaidi, S. El Atouani, C. Katif, F. Bentiss, C. Jama, A. Reani, B. Sabour, V. Vasconcelos, Isolation and FTIR-ATR and 1H NMR characterization of alginates from the main alginophyte species of the atlantic coast of Morocco, Molecules 25 (2020) 4335.

[53] S. Sahoo, C.K. Chakraborti, S. Naik, S.C. Mishra, U.N. Nanda, Structural analysis of ciprofloxacin-carbopol polymeric composites by X-Ray diffraction and Fourier transform infra-red spectroscopy, Trop. J. Pharm. Res. 10 (2011). https://www.ajol.info/index.php/tjpr/article/view/67938/0 (accessed July 29, 2025).

[54] S. Durgapal, S. Mukhopadhyay, L. Goswami, Preparation, characterization and evaluation of floating microparticles of ciprofloxacin, Int J Appl Pharm 9 (2017) 1–8.

[55] A.W. Chan, R.J. Neufeld, Modeling the controllable pH-responsive swelling and pore size of networked alginate based biomaterials, Biomaterials 30 (2009) 6119–6129.

[56] G. Pasparakis, N. Bouropoulos, Swelling studies and in vitro release of verapamil from calcium alginate and calcium alginate–chitosan beads, Int. J. Pharm. 323 (2006) 34–42. https://doi.org/10.1016/j.ijpharm.2006.05.054.

[57] V. Uskoković, Mechanism of formation governs the mechanism of release of antibiotics from calcium phosphate nanopowders and cements in a drug-dependent manner, J. Mater. Chem. B 7 (2019) 3982–3992.

[58] M. Fosca, J.V. Rau, V. Uskoković, Factors influencing the drug release from calcium phosphate cements, Bioact. Mater. 7 (2022) 341–363.

[59] N.S. Heredia, K. Vizuete, M. Flores-Calero, K. Pazmiño V, F. Pilaquinga, B. Kumar, A. Debut, Comparative statistical analysis of the release kinetics models for nanoprecipitated drug delivery systems based on poly (lactic-co-glycolic acid), PLoS One 17 (2022) e0264825.

[60] S. Dash, P.N. Murthy, L. Nath, P. Chowdhury, Kinetic modeling on drug release from controlled drug delivery systems, Acta Pol Pharm 67 (2010) 217–223.

[61] L.P. Jahromi, M. Ghazali, H. Ashrafi, A. Azadi, A comparison of models for the analysis of the kinetics of drug release from PLGA-based nanoparticles, Heliyon 6 (2020). https://www.cell.com/heliyon/fulltext/S2405-8440(20)30296-6 (accessed April 29, 2025).

[62] Y. Fu, W.J. Kao, Drug release kinetics and transport mechanisms of non-degradable and degradable polymeric delivery systems, Expert Opin. Drug Deliv. 7 (2010) 429–444. https://doi.org/10.1517/17425241003602259.

[63] J. Kolmas, P. Romaniuk, D. Predoi, A. Drobniewska, K. Burdan, B. Kołodziejska, Magnesium ion substitution in various calcium phosphates: A way towards bone regeneration, Ceram. Int. 51 (2025) 1153–1160.

[64] A.S. Abdul Rahman, A.N.S. Fizal, N.A. Khalil, A.N. Ahmad Yahaya, M.S. Hossain, M. Zulkifli, Fabrication and characterization of magnetic cellulose–chitosan–alginate composite hydrogel bead bio-sorbent, Polymers 15 (2023) 2494.

[65] W.L. Guerra-Ponce, S.L. Gracia-Vásquez, P. González-Barranco, I.A. Camacho-Mora, Y.A. Gracia-Vásquez, E. Orozco-Beltrán, L.A. Felton, In vitro evaluation of sustained released matrix tablets containing ibuprofen: a model poorly water-soluble drug, Braz. J. Pharm. Sci. 52 (2016) 751–759.

[66] K. Sinulingga, M. Sirait, N. Siregar, M.E. Doloksaribu, Investigation of Antibacterial Activity and Cell Viability of Ag/Mg and Ag/Zn Co-doped Hydroxyapatite Derived from Natural Limestone, ACS Omega 6 (2021) 34185–34191. https://doi.org/10.1021/acsomega.1c05921.

[67] K. Pajor, A. Michalicha, A. Belcarz, L. Pajchel, A. Zgadzaj, F. Wojas, J. Kolmas, Antibacterial and cytotoxicity evaluation of new hydroxyapatite-based granules containing silver or gallium ions with potential use as bone substitutes, Int. J. Mol. Sci. 23 (2022) 7102.

[68] F. Afhkami, P. Ahmadi, G. Rostami, Cytotoxicity of Different Concentrations of Silver Nanoparticles and Calcium Hydroxide for MC3T3-E1 Preosteoblast Cell Line, Clin. Exp. Dent. Res. 11 (2025) e70075. https://doi.org/10.1002/cre2.70075.

[69] L.S. Daniel, M.T. Joseph, V. Uahengo, M. Hedimbi, Antibacterial Activity of Visible Light Responsive-Silver-Nanoparticle/Titania Composite Thin Films with Unprecedently Higher Amounts of Silver, Adv. Mater. Interfaces 11 (2024) 2400035. https://doi.org/10.1002/admi.202400035.

[70] R. Cao, X. Zhai, X. Li, X. Zhao, Antibacterial properties of a novel nano-silver loaded poly(styrene-co-acrylic) composites, Polym. Polym. Compos. (2021). https://doi.org/10.1177/09673911211037499.

[71] M. Ghavam, Antibacterial potential of biosynthesized silver nanoparticles using Nepeta sessilifolia Bunge and Salvia hydrangea DC. ex Benth. extracts from the natural habitats of Iran's Rangelands, BMC Complement. Med. Ther. 23 (2023) 299. https://doi.org/10.1186/s12906-023-04101-w.

[72] M.A. Obeid, L. Akil, A.A. Aljabali, I. Khadra, Characterization of Ciprofloxacin-Loaded Polymeric Fiber Mats Prepared by Melt Electrospinning, Macromol. Mater. Eng. 309 (2024) 2300376. https://doi.org/10.1002/mame.202300376.

[73] M. Pahlevani, M. Beig, S.M. Barzi, M. Sadeghzadeh, M. Shafiei, M. Chiani, A. Sohrabi, M. Sholeh, S. Nasr, Antibacterial and wound healing effects of PEG-coated ciprofloxacin-loaded ZIF-8 nanozymes against ciprofloxacin-resistant Pseudomonas aeruginosa taken from burn wounds, Front. Pharmacol. 16 (2025). https://doi.org/10.3389/fphar.2025.1556335.

[74] M. Abu-Sini, M.A. Al-Kafaween, R.M. Al-Groom, A.B.M. Hilmi, M. Abu-Sini, M.A. Al-Kafaween, R.M. Al-Groom, A.B.M. Hilmi, Comparative *in vitro* activity of various antibiotic against planktonic and biofilm and the gene expression profile in *Pseudomonas*

aeruginosa, AIMS Microbiol. 9 (2023) 313–331. https://doi.org/10.3934/microbiol.2023017.

[75] M.M. Masadeh, K.H. Alzoubi, W.S. Ahmed, A.S. Magaji, In Vitro Comparison of Antibacterial and Antibiofilm Activities of Selected Fluoroquinolones against Pseudomonas aeruginosa and Methicillin-Resistant Staphylococcus aureus, Pathogens 8 (2019) 12. https://doi.org/10.3390/pathogens8010012.

Funding: This work was supported by the Medical University of Warsaw (WF6/N/25).

SERICIN-REINFORCED POLYSACCHARIDE COMPOSITES FOR POTENTIAL REGENERATIVE AND ANTIBACTERIAL APPLICATIONS

Barbara Kołodziejska[1*], Andrzej Pyzik[1], Ramona Figat[2], Julia Kopczyńska[3], Magdalena Kowalczyk[3], Joanna Kolmas[1]

[1]Department of Pharmaceutical Chemistry and Biomaterials, Faculty of Pharmacy, Medical University of Warsaw, Banacha 1 str., 02-097, Warsaw, Poland

[2]Department of Toxicology and Bromatology, Faculty of Pharmacy, Medical University of Warsaw, Banacha 1 str., 02-097, Warsaw, Poland

[3]Institute of Biochemistry and Biophysics, Polish Academy of Sciences, Pawińskiego 5A, 02-106 Warsaw, Poland

[*]**Corresponding Author**

Barbara Kołodziejska

Medical University of Warsaw

Faculty of Pharmacy

Department of Pharmaceutical Chemistry

ul. Banacha 1, 02-097 Warsaw, Poland.

Phone: +48 22 5720755

e-mail: barbara.kolodziejska@wum.edu.pl

Abstract

In this work, three polysaccharide matrices were prepared with varying chitosan-to-alginate weight ratios (70:30, 50:50, 30:70) and used to develop sericin-reinforced composite biomaterials loaded with ciprofloxacin and silver, either as nanoparticles or silver ions incorporated into nanocrystalline hydroxyapatite (AgHA). To obtain composites, a solid-liquid method was employed in combination with lyophilization. SEM analysis revealed highly porous structures with pore sizes ranging from 50 to 200 μm for silver nanoparticle composites and below 100 μm for AgHA-containing composites. Ciprofloxacin was loaded with high efficiency (95.2±1.1%), while silver loading efficiencies were 29.3±2.6% for nanoparticles and 20.4±1.3% for AgHA. In vitro release studies demonstrated biphasic ciprofloxacin release over 28 days, with initial diffusion-driven release followed by a slower phase (Korsmeyer-Peppas model, n = 0.035–0.070). Silver ions were released similarly, whereas silver nanoparticles exhibited zero-order kinetics in the second phase. Antimicrobial testing revealed significant activity against multidrug-resistant Staphylococcus aureus NCTC9789 and Pseudomonas aeruginosa PAO1161. Cytotoxicity assays confirmed that all composites were non-toxic to BALB/c 3T3 fibroblasts. These results indicate that the developed composites possess dual functionality—serving as temporary bone dressings for wounds and local drug delivery systems—offering sustained antibiotic release and prolonged antimicrobial protection, which may help to prevent infections associated with orthopedic implants.

Keywords: biomaterials, drug delivery, antibacterial activity, ciprofloxacin, composite

Introduction

Peri-implant infections, also known as Biomaterial-Associated Infections (BAIs), remain a significant challenge in reconstructive and restorative surgery, including dental and bone implantology, despite numerous preventive measures [1]. Bacterial colonisation of biomaterial surfaces, which initiates infection, can disrupt the functional integration of the biomaterial with bone tissue. The inflammation induced by the infection leads to resorption of the bone tissue surrounding the implant, ultimately resulting in poor implant-to-tissue integration and implant loss. A particularly challenging aspect of these infections is the formation of biofilms by bacteria, which confer significant resistance to many bactericidal agents. Systemic prophylactic antibiotic therapy is not always effective, largely due to poor drug penetration into inflamed, hypoxic tissues. Consequently, strategies such as intraoperative localised antibiotic administration are actively explored for more effective prevention [2,3].

The development of new antibiotics and antibacterial agents is a key priority for the World Health Organization (WHO) [4]. At the same time, traditional solutions, such as silver ions and nanoparticles, are being revisited due to their potent antibacterial activity. The antibacterial efficacy of silver has been recognised since antiquity, with no reports of bacterial resistance to date. Silver is currently being investigated for its effectiveness in treating infections caused by multidrug-resistant bacterial strains [5–8]. The bactericidal mechanism of silver involves interactions between silver ions and thiol (-SH) groups in bacterial proteins, leading to the substitution of hydrogen atoms and the formation of S-Ag bonds. This results in protein denaturation, deactivation of cellular pumps, membrane dysfunction, and the destruction of bacterial cell walls and membranes [6,9].

In bone tissue engineering, the current focus includes developing biomaterials, that not only fill bone defects or replace degraded tissue but also serve as carriers for drug delivery, such as antibiotics. Composite materials are particularly promising in fulfilling these dual roles and

offering appropriate biocompatibility, mechanical strength, enhanced tissue-implant integration, and prolonged, effective drug release [10–12].

Over the past two decades, significant attention has been directed towards materials of natural origin, including natural polymers, for composite development. Among these, alginate and chitosan have been extensively studied [13–20].

Chitosan, a linear polymer composed of randomly distributed β-(1,4)-D-glucosamine and N-acetyl-D-glucosamine units, commercially produced by deacetylation of chitin, a major component of crustacean exoskeletons and fungal cell walls. Chitosan exhibits excellent biocompatibility, biodegradability, and non-toxicity. Its chemical structure, particularly the presence of protonable amino groups along the D-glucosamine residues, accounts for most of its biological properties. These positively charged groups interact with negatively charged cell membranes, conferring hemostatic, mucoadhesive, antibacterial, and antifungal properties. Furthermore, chitosan's absorption capacity and ability to form porous, fibrous scaffolds make it suitable for controlled drug delivery systems and sustained-release applications [21,22].

Alginate, a biodegradable linear copolymer of β-D-mannuronate and α-L-guluronate molecules linked by β-1,4-glycosidic bonds, is primarily derived from seaweed and marine algae (e.g., *Laminaria hyperborea* and *Macrocystis pyrifera*). Alginic acid and its sodium salt form durable gels upon cross-linking with divalent cations, a property widely used in biomaterial engineering and medicine [23]. The hydrophilic nature of alginate gels makes them effective as wound dressings, capable of absorbing exudates and accelerating healing. Numerous studies highlight alginates' potential as carriers for controlled drug release [24].

In inorganic-organic bone composites, hydroxyapatite ($Ca_{10}(PO_4)_6(OH)_2$) is the most commonly used inorganic component. This material closely resembles biological apatite in composition and structure, a key component of the inorganic matrix in mineralised tissues (e.g., enamel,

dentin, and bone) [25–27]. Nanocrystalline hydroxyapatite offers excellent biocompatibility, osteoconductivity, non-toxicity, and immunogenicity, making it an exceptional bone substitute material with high potential for use as a drug delivery vehicle for direct application to bone tissue [28,29].

Our composites were reinforced with sericin, a globular protein present in silk produced by the *Bombyx mori* silkworm. Sericin contains numerous polar groups, enabling interactions with other polymers to improve mechanical properties and enhance the stability of biomaterials. Moreover, numerous studies have shown that sericin accelerates wound healing and collagen production with minimal immune response [30–33]. It also has a bactericidal effect and effectively inhibits the development of biofilm [34–36]. In osteoblast studies, sericin increased their proliferation and demonstrated regenerative effects on bone tissue [37–39].

Our research aimed to develop new polysaccharide composites reinforced with sericin, capable of releasing both the antibiotic and silver to ensure effective antibacterial activity. Until now, researchers worldwide have focused on developing biomaterials with a similar composition [40–43]; however, their primary objective was to design local wound dressings capable of delivering drugs with appropriate release kinetics. In contrast to these studies, our goal was to obtain a local dressing intended for application within bone tissue, which could be utilised in dentistry or for the treatment of minor bone defects, serving a preventive function by inhibiting the development of bacterial infections. It is of utmost importance to develop materials specifically targeted for bone tissue, as it is poorly vascularized; consequently, systemic pharmacotherapy is often insufficiently effective. We evaluated the efficacy of silver release in the form of nanoparticles and silver ions from Ag-substituted nanohydroxyapatite. The physicochemical properties of the composites were analysed, and the release profiles of both silver and antibiotic (ciprofloxacin) were examined. The antibacterial activity and cytotoxicity of the obtained materials were also studied.

Materials and Methods

Synthesis of hydroxyapatite containing silver ions (AgHA)

Hydroxyapatite containing silver ions was synthesized using the method described in detail by Pajor et al. [44]. Briefly, calcium nitrate tetrahydrate $Ca(NO_3)_2 \cdot 4H_2O$ (purity 99%) and silver nitrate ($AgNO_3$, assay ≥99.0%) were used as sources of calcium and silver ions, respectively, and were dissolved in distilled water. Then, an ammonium hydrogen phosphate solution ($(NH_4)_2HPO_4$, assay ≥98%) was introduced dropwise in such an amount that the (Ca+Ag)/P molar ratio was 1.67 and stirred on a magnetic stirrer. All the reagents were of analytical grade and purchased from Sigma Aldrich Chemicals, St. Louis, MO, USA. After mixing the solutions, a white precipitate formed. Then, the flasks with the suspension were left with the stirrer on for another 1 hour, and then the suspension was made alkaline with a 25% NH_4OH solution (≥99.99% trace metals basis), adjusting the pH to approximately 11. In the next stage, the mixing was turned off and the precipitate in the mother solution was left for 24 hours to age (so-called precipitate maturation). After 24 hours, the obtained apatites were centrifuged and rinsed several times with distilled water until the pH reached ~ 7. After centrifugation, the precipitate was filtered under reduced pressure and then dried at 100°C for 24 hours. After drying, the obtained precipitate was micronized using an agate mortar. Subsequently the powder was sieved through a <40 μm mesh to eliminate hard agglomerates and subjected to further tests. For comparison, the pure, unsubstituted hydroxyapatite (HA) was obtained in the same conditions.

The identity of the obtained powders was examined using the powder X-ray diffraction (PXRD) method. A Bruker D8 Discover diffractometer equipped with a position detector and Cu-Kα radiation (λ = 0.15418 nm) was used. The measurements used the horizontal Bragg–Brentano (θ/θ) geometry (plane reflection mode) in the range from 15° to 60° (2θ) in a continuous scan, using steps of 0.03° and 2 s/step (total time 384 s/step). The identification of crystalline phases

was obtained by comparing the obtained diffractograms of HA and Ag-HA samples with the standard reference (JCPDS 09-0432). The mid-infrared FT-IR spectroscopy method in the transmission technique (using a KBr pellet) was used to analyse the chemical structure of hydroxyapatites. FT-IR spectra were recorded on a Shimadzu spectrometer with a resolution of 2 cm^{-1}, in the 4000-400 cm^{-1} range. Each measurement was performed using 30 scans. The crystal morphology was analysed by transmission electron microscopy (TEM) using the high-performance JEM 1400 transmission electron microscope (TEM-JEOL Co., Tokyo, Japan, 2008), equipped with Morada G2 TEM camera (EMSIS GmbH, Germany) under an accelerating voltage of 80 kV. Sample preparation consisted of dropping a suspension of the tested powder previously prepared in ethanol onto a Formvar grid. The silver content of the hydroxyapatite sample enriched in silver ions was measured using the F-AAS method (ANALYST 400, Perkin Elmer, Llantrisant, UK, with detection at a wavelength of $\lambda = 328.07$ nm). For this purpose, the sample was dissolved in super-pure concentrated nitric acid (63% HNO_3) and appropriately diluted with deionized water. The calibration curve was prepared by dissolving an appropriate amount of calibration $AgNO_3$ standard in deionized water (Avantor Performance Materials, Gliwice, Poland).

Preparation of composites

To obtain composites, the following reagents were prepared: chitosan (medium molecular weight, 75–85% deacetylation degree, viscosity ≤ 300 cP, Sigma-Aldrich, Burlington, MO, USA), sodium alginate (Sigma Aldrich, Burlington, MO, USA), sericin from *Bombyx mori* (silkworm, Sigma Aldrich, Burlington, MO, USA), glycerin (Sigma Aldrich, Burlington, MO, USA), silver nanoparticles (5 nm particle size, 5 mg/mL, silver nanospheres, in 2mM aqueous sodium citrate, nanoComposix), and hydroxyapatite enriched with silver ions (AgHA). A 3 wt.% suspension of alginate and chitosan was prepared in distilled water and combined in three different weight ratios of 30:70, 50:50, and 70:30. To 80 mL of each mixture obtained in this

way, 8 drops (~0.4 mL) of pure glycerin (≥99.5%) and 1.0 mL of sericin solution was added (prepared by dissolving 0.1 g of *Bombyx mori* sericin powder in 1.0 mL of distilled water under gentle stirring to ensure complete dissolution). After thorough mixing, 3.6 g of AgHA or 0.4 mL of silver nanoparticle suspension was added (in both cases, the amount corresponded to 6 mg of silver per 1 gram of composite). Since no aggregation-inducing conditions were introduced during the composite preparation, the size of nanoparticles was assumed to remain comparable to that in the free form. Finally, 145 mg of ciprofloxacin was added to the obtained thick suspension (the amount corresponds to 100 mg of ciprofloxacin per 1 g of the composite). All obtained suspensions were poured into Petri dishes. Then the dishes were frozen at -80°C and lyophilised for 48h. Freeze-dried samples were cross-linked using first 1.5% $CaCl_2$ solution (cross-linking for 10 min) and then 1M NaOH solution (cross-linking for 10 min). After cross-linking, the samples were rinsed three times for 15 min in distilled water and subjected to freezing and lyophilisation again. The solutions obtained after cross-linking and rinsing were collected in tubes to determine the ciprofloxacin content released during cross-linking and rinsing. As a result of the above procedures, six different composites were obtained, differing in the alginate-to-chitosan ratio and the form of incorporated silver (nano-Ag and AgHA). The list of obtained samples is presented in Table 1.

Table 1. Types of obtained composites.

Sample	**C1AgHA**	**C1Ag-n**	**C2AgHA**	**C2Ag-n**	**C3AgHA**	**C3Ag-n**
Polymer ratio (alginate: chitosan)	**30:70** (24 mL of 3% alginate and 56 mL of 3% chitosan)		**70:30** (56 mL of 3% alginate and 24 mL of 3% chitosan)		**50:50** (40 mL of 3% alginate and 40 mL of 3% chitosan)	
Glycerin	0.4 mL	0.4 mL	0.4 mL	0.4 mL	0.4 mL	0.4 mL

Sericin	1.0 mL of 10% solution	1.0 mL of 10% solution	1.0 mL of 10% solution	1.0 mL of 10% solution	1.0 mL of 10% solution	1.0 mL of 10% solution
Hydroxyapatite doped with silver	3.6 g	-	3.6 g	-	3.6 g	-
Silver nanoparticles	-	0.4 mL of 5 mg/mL	-	0.4 mL of 5 mg/mL	-	0.4 mL of 5 mg/mL
Ciprofloxacin	145 mg	145 mg	145 mg	145 mg	145 mg	145 mg

Studies of the obtained composites

To assess the porosity and topographic structure of the surface of the obtained composites, the samples were examined by scanning electron microscopy (SEM, Nova NanoSEM 200, Fei).

The mid-infrared FT-IR spectroscopy method in the attenuated total reflectance (ATR-FTIR) technique was used to analyse the chemical structure of all composites. FT-IR spectra were recorded on a Shimadzu IRAffinity-1S spectrometer in the 4000–400 cm^{-1} range. Each measurement was performed using 150 scans.

The swelling test was performed using the standard gravimetric method. Firstly, the lyophilised samples were weighed (initial weight, W_0). Then, the samples were immersed in phosphate-buffered saline (PBS; pH 7.4) at 37 °C. At predetermined time intervals (15 minutes, 30 minutes, 1 hour, 3 hours, 5 hours, 12 hours, 24 hours and 48 hours) the samples were removed from the solution, wiped dry with filter paper to remove excess liquid from the surface, and weighed again.

To calculate the swelling ratio at time t, the following equation was used:

$$\%SR = \frac{(Wt-W_0)}{W_0} \times 100 \quad (1)$$

where W_0 and W_t are the weights of the initial dry and swollen samples at fixed time intervals t, respectively. All the measurements were performed in triplicate.

The study of ciprofloxacin and silver release from the obtained composites was carried out using the HPLC method and the F-AAS method, respectively. The prepared composite samples, in the form of cylindrical discs with a diameter of 15 mm, a height of 10 mm, and a mass of 300 mg were placed in falcon test tubes, to which 50 mL of distilled water was added. The test tubes were placed in a shaker and incubated at 37°C while slowly mixing to ensure conditions similar to physiological conditions. The shaking frequency was set at 50 rpm. Samples of the incubation media were taken first after 15 and 30 minutes, then after 1, 3, 6, 12, 24, 48 and 72 hours and then after 7, 14, 21 and 27 days. Before each collection, the contents of the test tubes were mixed thoroughly, then 10 mL of the solution was taken using a syringe, filtered into a new test tube using membrane filters and, finally, the test tubes with composite samples were filled with the same volume of distilled water. Ciprofloxacin release was studied using the HPLC method. Sample analysis was performed on an RP-18 column (HPLC Column 250 x 4.6 mm x 1/4'' Microsorb-MV 100-5 C18), which was thermostated in a CTO-10ASVP oven from Shimadzu. The analysis was performed in a reverse phase system, using a mixture of phosphate buffer with pH = 3 and acetonitrile in a volume ratio of 80:20 as the mobile phase. The eluent flow rate was 1 mL/min. The chromatograph was connected to a UV-Vis detector (Varian Prostar 325). Each time, 20 µl of the solution was introduced into the column. Before starting the sample measurements, a calibration curve was prepared using standard solutions. Absorbance was measured at a wavelength of 278 nm. To investigate the release profile of silver from the composites, the F-AAS method (PerkinElmer AAnalyst 400 AA Spectrometer) was used at a wavelength of 328 nm, after preparing a calibration curve.

To evaluate the release mechanism and kinetics of ciprofloxacin and silver, the experimental data were fitted to several mathematical models commonly used to describe drug release from polymeric and composite matrices.

Zero-order model:

$$\frac{Q_t}{Q_\infty} = k_0 t \quad (2)$$

First-order model:

$$\log(1 - \frac{Q_t}{Q_\infty}) = -k_1 t / 2.303 \quad (3)$$

Higuchi model:

$$Q_t / Q_\infty = k_H t^{1/2} \quad (4)$$

Korsmeyer–Peppas model (K–P model):

$$\frac{Q_t}{Q_\infty} = k_{KP} t^n \quad (5)$$

Peppas–Sahlin model:

$$\frac{Q_t}{Q_\infty} = k_1 t^n + k_2 t^{2n} \quad (6)$$

Weibull model:

$$\frac{Q_t}{Q_\infty} = 1 - \exp[-(\frac{t - T_i}{\tau})^\beta] \quad (7)$$

Where k_0, k_1, k_2, k_H, k_{KP}, τ refer to the rate constants, Q_t/Q_∞ represents the fraction of the drug released at a time t, n refers to the diffusion coefficient, Ti - the lag time before release onset, and β is the shape parameter. Depending on the value of β, the release profile may be exponential ($\beta = 1$), parabolic ($\beta < 1$), or sigmoidal ($\beta > 1$) [45,46].

All models were fitted to the experimental data using nonlinear regression. The coefficient of determination (R^2) was used to evaluate the goodness of fit. Model equations and parameters were implemented in Kaleidagraph 5 (Synergy Software).

The cytotoxicity of the materials was evaluated in accordance with ISO 10993-5:2009 guidelines [47] by the neutral red uptake (NRU) assay and MTT assay, using the mice fibroblast cell line BALB/c 3T3 clone A31 (American Type Culture Collection). Due to the observed high liquid absorption of the samples, the volume of extraction medium absorbed by each 100 mg of material was determined in accordance with ISO 10993-12:2012 protocol prior to extract

preparation. This additional volume was then added to every 100 mg in the extraction mixture during extraction of the material. The highest extract concentration tested was 50 mg/mL. The materials were UV-sterilized using UV-C light at a wavelength of 254 nm for 30 minutes, ensuring uniform exposure by gentle mixing of the powder several times during the process. The extracts were sterilized by filtration using a filter with a pore size of 0.2 µm. Extracts were prepared by incubating the samples in DMEM medium with 5% bovine serum for 24 hours at 37 ◦C with stirring. The extracts were sterilized by filtration. The cells were treated with seven dilutions of each extract in a two-dilution series for 24 hours. Highly cytotoxic latex and non-cytotoxic polyethylene film were used as reference materials. A material is considered to have cytotoxic potential when the cell viability is less than 70%. In our study, the experiments were performed in triplicate ($n \geq 3$). The data are presented as mean values ± SD.

Antimicrobial activity

The antimicrobial activity of the composites was tested against *Staphylococcus aureus* NCTC9789 and *Pseudomonas aeruginosa* PAO1161 from the IBB strain collection. This was assessed via the disk diffusion method, where bacterial suspensions of 0.5 McFarland standard were streaked in three different directions on 60 mL Mueller-Hinton agar. Then, the composites were placed on the streaked plate and co-incubated with bacteria for 24 hours at 37 °C. After the incubation time, the zone of growth inhibition was measured. Statistical analysis was performed by GraphPad Prism 10.4.2. Normality was tested using the Shapiro-Wilk test and group comparison was carried out by one-way ANOVA with Dunnett post-hoc test.

Results and Discussion

Physicochemical parameters of AgHA powder

The first step involved the synthesis of hydroxyapatite enriched with silver ions, intended to serve as a source of silver in some of the composites. Figure 1S in the Supplementary Materials presents the results of physicochemical studies for the AgHA powder and the reference material (non-substituted HA). All reflections in both PXRD patterns confirm the successful synthesis of hydroxyapatite (compared to JCPDS 09-0432) and the absence of other crystalline phases. The reflections in the AgHA diffractogram are broad and diffuse, typical for weakly crystalline materials. Crystallite size parameters calculated using the Scherrer formula along the *a* and *c* axes indicate that both materials are nanocrystalline, with crystals elongated along the *c* axis. This feature is observed in both the HA and AgHA samples (HA: 35±4 nm/16 ± 3 nm; Ag-HA: 26±4 nm/8 ±2 nm). FT-IR spectra further confirm the nanocrystalline nature of the obtained materials. The poor resolution of the ν_4 band of orthophosphates in the 650–500 cm^{-1} range in both spectra, along with a very weak band corresponding to structural hydroxyl groups at 3570 cm^{-1}, supports this conclusion. Additionally, the $\nu_1+\nu_3$ bands of orthophosphates are broad and less resolved in the spectrum of the AgHA sample, corroborating its lower crystallinity compared with the HA sample.

TEM images (Figure 1S) show small, elongated crystals of the synthesized materials, typically compacted into large agglomerates. According to the literature, incorporating silver ions into the hydroxyapatite structure reduces crystallinity, suggesting their successful into the crystal lattice [44]. The silver content in the AgHA sample, as determined by the F-AAS method, is 0.25 wt.%, which corresponds to 83% of the nominal amount introduced.

SEM microscopy

Cross-sectional SEM images of the obtained matrices are shown in Figure 1. All samples exhibit very high porosity across the entire analysed surface. The pores are interconnected and display irregular shapes and sizes, which is typical for polysaccharide materials subjected to freezing and lyophilization processes. Samples without hydroxyapatite (Figures C1Ag-n, C2Ag-n, C3Ag-n) exhibit a fibrous structure with relatively large pores ranging from 50 to 200 µm. High-magnification images reveal the presence of silver nanoparticles deposited on the surface of the fibers (marked with red arrows) [48].

Figure 1. SEM images of all obtained composites.

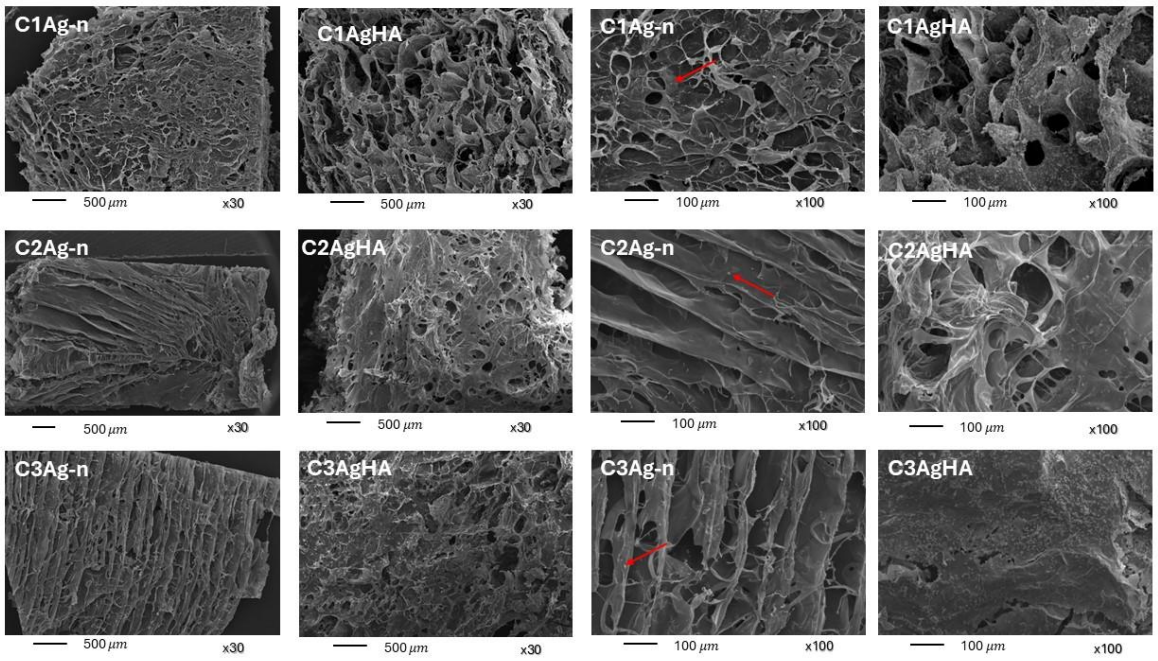

The ultrastructure of composites containing Ag-HA appears slightly more compact and dense, resembling a sponge. Hydroxyapatite is deposited on the polymer fibers and partially fills the structure, effectively reducing porosity (with pore sizes not exceeding 100 µm). Additionally, it is observed that samples with the highest chitosan-to-alginate weight ratio (C1AgHA and C1Ag-n) exhibit a relatively disordered network and irregular structure, alongside higher porosity. This may indicate the formation of more random networks during the freezing process.

ATR-FTIR analysis

The FT-IR spectra of all obtained composites and their individual components are provided in the supplementary materials (Figures 2S and 3S). Figure 2S shows the spectra of composites containing silver-doped hydroxyapatite (AgHA). By analyzing the spectra of the individual components, the presence of hydroxyapatite in all samples can be confirmed, as well as the presence of the respective polymers and ciprofloxacin. The detailed band assignments are presented below. Characteristic hydroxyapatite bands appear around 1100, 1040, 870, 610, and 560 cm^{-1}. The bands at 1100 and 1040 cm^{-1} correspond to phosphate stretching vibrations, while the band at 870 cm^{-1} is attributed to bending vibrations of carbonate groups (CO_3^{2-}) substituting phosphate groups. Bands near 610 and 560 cm^{-1} represent phosphate bending modes.

Bands observed at 2930, 1603, 1410, 1305, and 820 cm^{-1} are mainly attributed to alginate, which is the major component of the composite. The 2930 cm^{-1} band corresponds to -CH stretching, 1603 and 1410 cm^{-1} to asymmetric and symmetric stretching of -O-C-O groups and bending of -C-OH, 1305 cm^{-1} to -C-C-H and -O-C-H bending within the pyranose rings, and 820 cm^{-1} to mannuronic acid residues.

Additional bands at 2865, 1650, and 1170 cm^{-1} indicate the presence of chitosan. These correspond to -CH_2 stretching (2865 cm^{-1}), amide -C=O stretching (1650 cm^{-1}), and -C-O-C stretching vibrations (1170 cm^{-1}).

Moreover, characteristic bands of ciprofloxacin are visible at 1270 and 805 cm^{-1}, associated with -C-F stretching and aromatic ring vibrations, respectively, confirming its presence in the composites.

Analysis of the FT-IR spectra of composite samples containing silver nanoparticles (Figure 3S) reveals the presence of intense, broad bands in the 1170–940 cm^{-1} region, which result from overlapping signals characteristic of alginate and chitosan.

As shown by comparison with literature data for the characteristic bands of the individual components [49–54], not all expected bands are visible in the recorded spectra. This is because some bands appear within the same wavenumber range; therefore, more intense bands may overshadow those with lower intensity. Nevertheless, the spectral analysis confirms that the obtained composites are composed as intended, comprising an organic phase of natural polymers, an inorganic hydroxyapatite phase, and the antibiotic ciprofloxacin.

Swelling behaviour

A parameter closely associated with the porosity and ultrastructure of biomaterials is the swelling coefficient. In this study, the swelling behaviour was evaluated at pH 7.4 and a temperature of 37 °C to closely mimic the physiological conditions of the bone tissue environment. Notably, porous matrices with swelling capability are highly effective for both bone tissue regeneration and reconstruction. This is due to their ability to facilitate fluid flow within swollen pores, ensuring nutrient mass transfer to cells while aiding in the removal of metabolic waste. Furthermore, swelling biomaterials can serve as carriers for drug substances and other biologically active compounds, primarily due to enhanced diffusion properties [55].

Figure 2 presents the swelling results for all tested materials over a 48-hour period. The samples exhibited variability in both the degree of swelling and the rate at which this process occurred. Materials with higher chitosan-to-alginate ratios demonstrated lower swelling capacities (absorption of aqueous solution), which can be attributed to the reduced hydrophilicity of chitosan compared to alginate. Additionally, the findings reveal that the incorporation of hydroxyapatite in the composites significantly reduces their swelling capacity [56].

Consequently, the sample with the lowest swelling coefficient was C1AgHA (approximately 382%), whereas the highest swelling capacity was observed for C2Ag-n (1170%).

Figure 2. Swelling test. The graph shows the swelling ratio (%) of the obtained materials at different times.

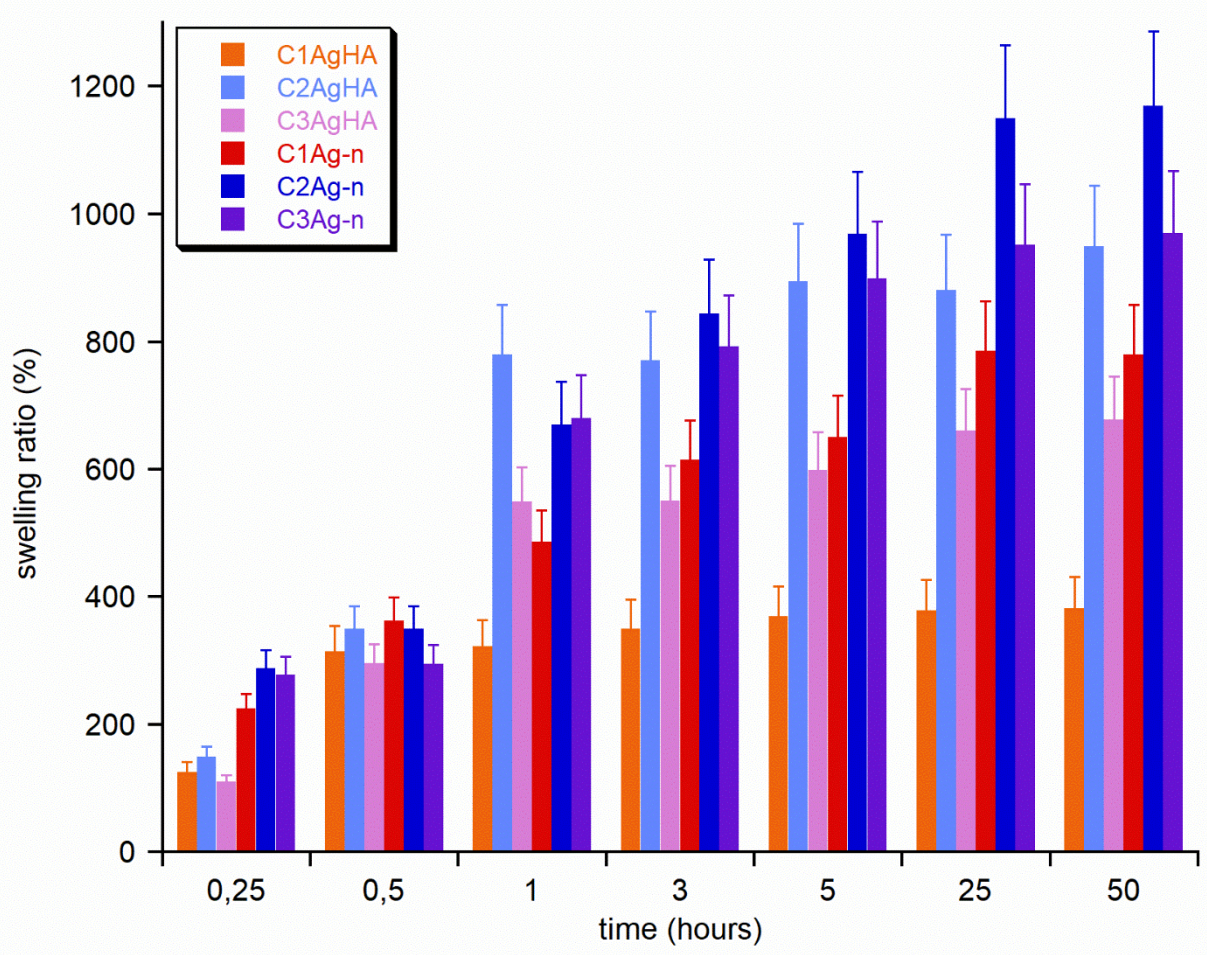

Antibiotic release

The ciprofloxacin loading efficiency was determined to be 95.2±1.1% across the tested composite. The evaluation of drug loading efficiency was made possible by quantifying the loss of ciprofloxacin during the cross-linking and rinsing processes of the composite suspensions. This loss corresponded to 4.8±1.1% relative to the total amount of drug introduced per composite, i.e. 100 mg of ciprofloxacin per 1 g of the composite. The HPLC chromatograms

(Figure 4S in Supplementary Materials) of the drug substance after 28 days confirmed the chemical stability of ciprofloxacin, showing consistent retention times and peak shapes comparable to the reference standard, with no evidence of degradation products.

The ciprofloxacin release profiles from each matrix are depicted in Figures 3a and 3b. All curves exhibit relatively similar release patterns, differing primarily in the quantity of drug released. Hydroxyapatite demonstrates the most pronounced effect on ciprofloxacin release, as its presence in the material significantly attenuates drug release. This effect may be attributed to the adsorption of ciprofloxacin molecules onto hydroxyapatite crystals through intermolecular interactions, such as van der Waals forces or the reduction in porosity within hydroxyapatite-containing materials [57,58].

Figure 3. Ciprofloxacin release profiles from the composite matrices: full release curves over 672 hours (a), initial release phase - first 48 hours (b); representative model fittings to Korsmeyer-Peppas model for C3AgHA in the short- and long-term release ranges (c, d – respectively).

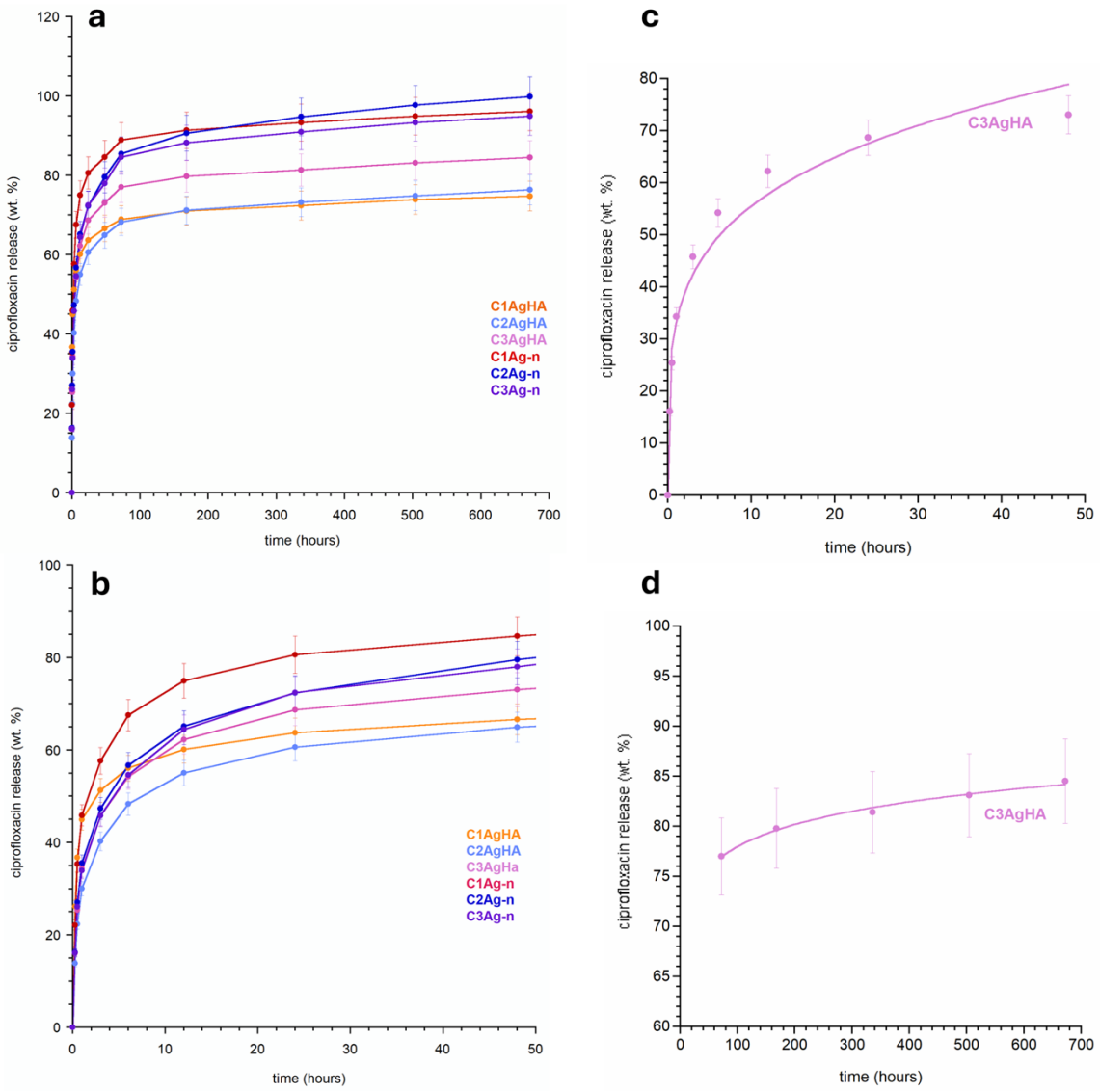

The experimental data were fitted to various mathematical models of drug release, including the zero-order, first-order, Higuchi, Korsmeyer-Peppas (K-P), Weibull, and Peppas-Sahlin models [59–61]. The Peppas–Sahlin and Weibull models were preliminarily tested using one representative release profile. However, the obtained fitting parameters and curve shapes were inconsistent with the experimental data and the biphasic character of the release process. Therefore, these models were not further applied to all samples and were excluded from the main analysis.

Representative fitting parameters and R^2 coefficients for selected ciprofloxacin release models for one sample are presented in Table 1S in the Supplementary Materials.

A detailed analysis indicated that the K-P model provided the best fit, dividing the release into two phases: an initial phase up to 48 hours and a subsequent phase spanning 48 to 672 hours. The K-P model is frequently used to characterize the release of active substances from carriers such as hydrogels, polymer films, and biomaterial composites [60]. The fitting data, presented in Table 2, reveal that in the first phase, the release mechanism is predominantly diffusion-driven but atypically slow compared to standard Fickian diffusion ($n<0.45$). The second phase is characterized by an even lower n value ($n \ll 0.45$, specifically $n=0.035-0.070$), suggesting extremely slow diffusion. When n approaches zero, the release approximates zero-order kinetics, maintaining a nearly constant rate over time.

In these matrices, the observed slowing of release may result from the depletion of ciprofloxacin in readily accessible regions, leading to a significant reduction in the concentration gradient. The increased k_{KP} value during this phase (nearly doubling for each sample) suggests the involvement of additional release mechanisms, potentially linked to matrix relaxation and polysaccharide swelling, particularly alginate [58,61,62]. These complex mechanisms warrant further investigation.

Table 2. Summary of fitting parameters for ciprofloxacin and silver release.

	Ciprofloxacin release							
Sample	I phase (0-48 hours)				II phase (48-672 hours)			
	k_{KP}	n	R^2	Model	k_{KP}	n	R^2	model
C1AgHA	8.7±0.4	0.14±0.01	0.9840	K-P	12.5±0.1	0.036±0.001	0.9955	K-P
C2AgHA	7.1±0.5	0.23±0.02	0.9831	K-P	13.4±0.1	0.048±0.002	0.9975	K-P
C3AgHA	9.4±0.6	0.22±0.02	0.9833	K-P	18.3±0.2	0.040±0.002	0.9947	K-P
C1Ag-n	15.0±0.9	0.19±0.02	0.9799	K-P	26.5±0.2	0.035±0.001	0.9980	K-P
C2Ag-n	15.4±0.9	0.23±0.02	0.9868	K-P	28.5±0.2	0.070±0.001	0.9996	K-P
C3Ag-n	13.6±0.8	0.23±0.02	0.9877	K-P	27.9±0.3	0.051±0.002	0.9982	K-P
	Ag release							
	I phase (0-48 hours)				II phase (48-672 hours)			
C1AgHA	6.0±0.4	0.17±0.02	0.9604	K-P	8.8±0.3	0.058±0.005	0.9885	K-P
C2AgHA	1.04±0.04	0.23±0.02	0.9905	K-P	1.6±0.2	0.14±0.02	0.9627	K-P
C3AgHA	2.2±0.1	0.27±0.02	0.9850	K-P	4.1±0.2	0.107±0.007	0.9944	K-P
					Q_0	k	R^2	
C1Ag-n	1.06±0.04	0.24±0.01	0.9921	K-P	2.16±0.06	0.012±0.001	0.9998	Zero order
C2Ag-n	3.3±0.2	0.21±0.03	0.9671	K-P	7.2±0.2	0.0029±0.0004	0.9682	Zero order
C3Ag-n	1.64±0.08	0.28±0.02	0.9937	K-P	4.8±0.20	0.0154±0.0005	0.9984	Zero order

Silver Release

Similar to ciprofloxacin, the loading efficiency of silver nanoparticles and the silver content incorporated into HA within the composites were also determined. In contrast to ciprofloxacin, significant losses of silver occurred during the cross-linking and rinsing of the composite suspensions. The loading efficiency of silver nanoparticles was 29.3±2.6% whereas the efficiency of silver incorporation in HA-containing composites amounted to 20.4±1.3%. The experimental curves depicting silver release from the composites are analyzed in a similar manner. Figure 4a presents the experimental release profiles for all matrices, while Figures 4b-c and 4d-e detail the fits for samples containing hydroxyapatite enriched with silver ions or silver nanoparticles, respectively. Representative fitting parameters and R^2 coefficients for selected Ag^+ release models for two samples are presented in Table 2S in the Supplementary Materials.

Figure 4. Silver release profiles from all composite matrices (a), model fitting results for materials with silver-ion-doped hydroxyapatite (b–c), fitted release curves for composites containing hydroxyapatite with embedded silver nanoparticles (d–e).

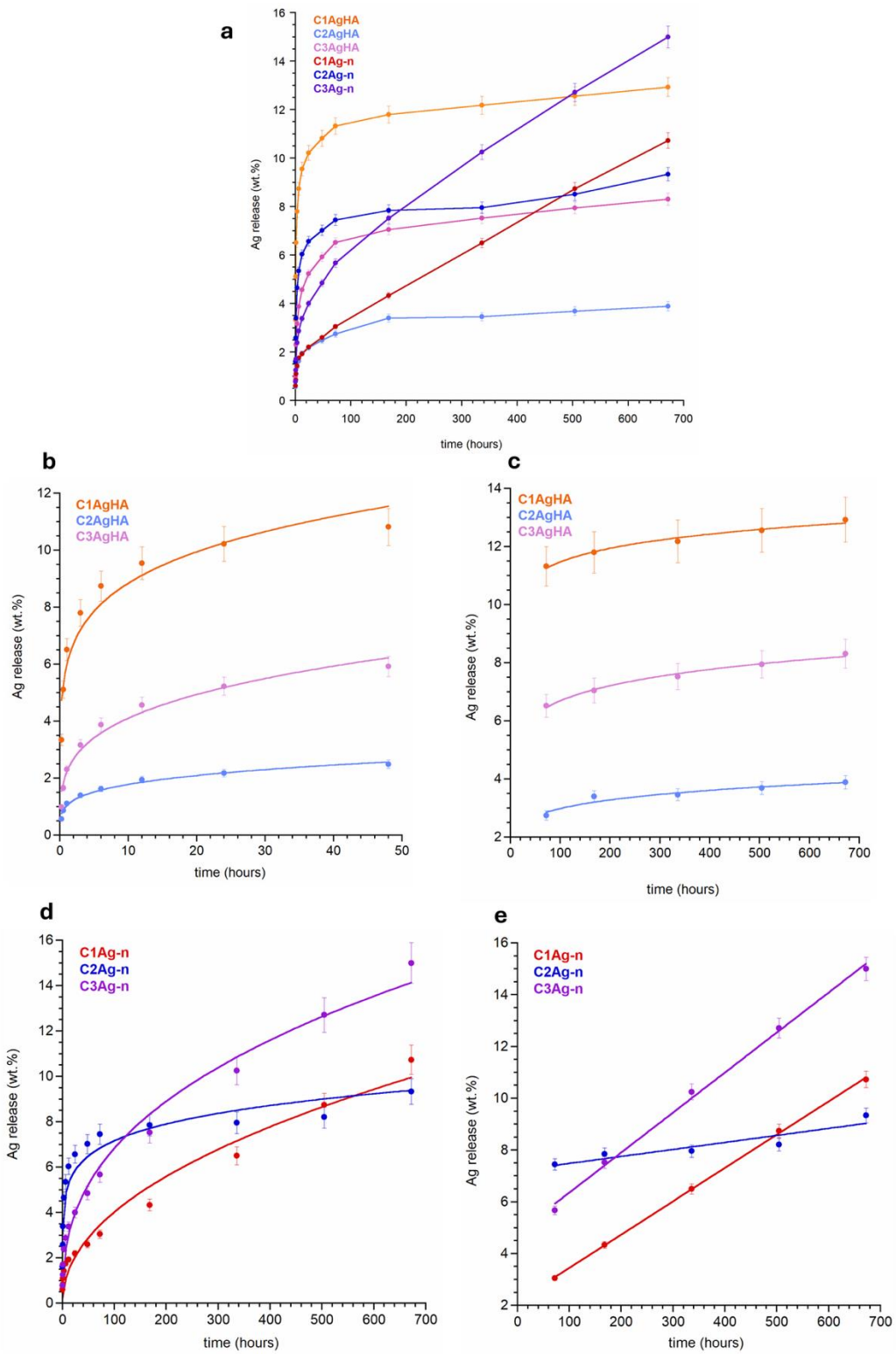

In contrast to ciprofloxacin release, which reaches 75–99% within 28 days (depending on the sample), the silver release profiles indicate markedly slower release rates, ranging from 4% to 15%. Previous studies on ion release (e.g., selenium, zinc, silver, and gallium) from nanocrystalline hydroxyapatite and various composite matrices have similarly demonstrated slow release over comparable timeframes (4–5 weeks) relative to drug substances [20,44,63]. This may result from strong interactions between ions/nanoparticles and the matrix components, particularly alginate and/or chitosan. For example, silver ions may bind to negatively charged groups within the alginate matrix, while in chitosan matrices, complexes may form between silver ions and amine groups [64]. Such binding can impede ion release, causing significant delays.

Figures 4b and 4c suggest that silver ions exhibit stronger binding to alginate than to chitosan. A similar trend is observed for silver nanoparticles (Figures 4d and 4e). The fitting parameters for silver release are summarized in Table 2. The data suggest that, similar to ciprofloxacin, the silver release process can be divided into two distinct phases, with a transition point at 48 hours.

During the first phase, all curves fit well to the K-P model, with n-values ranging from 0.17 to 0.28, indicating Fickian diffusion. In the second phase (48–672 hours), the release of silver ions from hydroxyapatite-containing matrices is also best described by the Korsmeyer-Peppas model. However, as with ciprofloxacin, the diffusion process is significantly restricted ($n=0.058-0.14$).

For samples C1Ag-n, C2Ag-n, and C3Ag-n (containing nanoparticles), the release data in the second phase can be accurately described ($R^2=0.9682-0.9998$) using the zero-order kinetics model [59,65]. In this phase, silver ion release occurs at a constant rate, independent of concentration. The zero-order release observed in the second phase may be associated with matrix swelling, relaxation, and reduced nanoparticle-matrix interactions [61].

The biphasic release profiles observed for ciprofloxacin and silver species can be correlated with the hydration behaviour of the matrices. Rapid water uptake during the initial hours promoted the swelling of the polysaccharide network, increasing the diffusion pathways for drug molecules. As the system reached equilibrium hydration, the matrix structure became denser due to partial gelation and polymer rearrangement, which limited further diffusion and resulted in a slower release rate.

Cytotoxicity Assay

Table 3 shows the results of the MTT and NRU test for the highest tested concentration for the silver-doped hydroxyapatite (AgHA) and silver nanoparticle (Ag-N) composites. According to the NRU and MTT test methodologies, none of the seven tested dilutions of either material extract was classified as cytotoxic, since no decrease in cell viability was observed in either of the two cytotoxicity assessment tests (Table 3S and 4S). These results indicate that both silver-doped hydroxyapatite composites (AgHA) and silver nanoparticles (Ag-N) composites are biocompatible with the normal cells used in the tests, suggesting that the applied production process and concentrations maintain cell viability and do not cause cytotoxic effects. Similar findings were reported by Sinulingga et al. [66], who showed that silver and magnesium or zinc co-doped hydroxyapatite did not significantly reduce the viability of MC3T3-E1 cells in MTT assay performed according to ISO 10993-5, while providing strong antibacterial properties. On the other hand, slight cytotoxicity was observed in a publication from our team [67], where silver ion-doped hydroxyapatite granules showed reduced cell viability at higher concentrations in standard cell lines, indicating some cytotoxic potential. Additionally, Afhkami et al. [68] reported slight decreases in MC3T3-E1 preosteoblast viability after exposure to silver nanoparticles. These different outcomes show that the biocompatibility of silver-containing biomaterials depends on factors such as the concentration of silver, the form of the nanoparticles and the production methods used.

Table 3. MTT and NRU test results for the highest concentrations of test extracts (50 mg/mL) compared to the untreated control.

Sample	MTT test - cells viability ± SD (%)	NRU test - cells viability ± SD (%)	Classification
C1AgHA	114 ± 1	109 ± 5	Non-cytotoxic
C1Ag-n	118 ± 13	106 ± 15	Non-cytotoxic
C2AgHA	111 ± 4	94 ± 7	Non-cytotoxic
C2Ag-n	115 ± 4	102 ± 8	Non-cytotoxic
C3AgHA	139 ± 4	113 ± 5	Non-cytotoxic
C3Ag-n	121 ± 15	94 ± 13	Non-cytotoxic
LT	2 ± 3	3 ± 2	Cytotoxic
PE	113 ± 3	99 ± 1	Non-cytotoxic

LT—latex, reference cytotoxic material. PE—polyethylene film, reference non-cytotoxic material. SD—standard deviation. A decrease in the cell viability below 70% classifies the sample as cytotoxic.

Microbiology

The disc diffusion method was used to assess the antimicrobial activity of composites enriched with silver ions against the multi-drug-resistant bacterial strain *S. aureus* NCTC9789 and *P. aeruginosa* PAO1161. The zone of growth inhibition was measured and compared between the composites and controls. All of the composites exhibited significant antimicrobial activity against both pathogenic strains (Table 4). The largest zone of inhibition for *S. aureus* NCTC9789 was observed for the composites C2AgHA, C3Ag-n and C1Ag-n, respectively, however, the zone of inhibition for all composites ranged from 2.6-3.2 cm. In turn, for *P. aeruginosa* PAO1161, a higher antimicrobial activity of the composites was observed, measuring 3.3-3.7 cm of the zone of growth inhibition. The highest inhibition of growth for this pathogen was shown for the composites C3AgHA, C1AgHA and C2AgHA.

Table 4. Zone of growth inhibition for pathogenic strains. Results are shown as mean ± SD (n=3). The values for the zone of growth inhibition are presented in cm. C1 and C3 are control composites, lacking antibiotics and silver ions (chitosan and alginate matrices). The statistical difference between control and treatment is presented by **** p<0.0001.

Composite/strain	*S. aureus* NCTC9789	*P. aeruginosa* PAO1161
C1Ag-n	3.0 ± 0.2 ****	3.3 ± 0.3 ****
C2AgHA	3.2 ± 0.2 ****	3.6 ± 0.2 ****
C1AgHA	2.9 ± 0.4 ****	3.7 ± 0.2 ****
C3Ag-n	3.2 ± 0.2 ****	3.5 ± 0.3 ****
C2Ag-n	2.8 ± 0.2 ****	3.5 ± 0.1 ****
C1	0 ± 0	0 ± 0
C3AgHA	2.6 ± 0.1 ****	3.7 ± 0.1 ****
C3	0 ± 0	0 ± 0

In the literature, several studies have reported microbiological results for materials containing silver or ciprofloxacin, demonstrating their well-established antibacterial potential. When it comes to silver nanoparticles, 11.2 to 18.8 mm inhibition zone was shown against *E. coli* with the increase of Ag-NPs content (%) in the composite films [69]. Nano-silver loaded poly(styrene-co-acrylic) (nAg-PSA) composites had maximum diameters of inhibition zones against the *E. coli* (1.18 mm) and *S. aureus* (1.29 mm) [70] and other studies confirm an inhibition zone of nanoparticles up to around 20 mm [71].

For ciproflaxin-loaded composites, e.g. ciprofloxacin-loaded polymeric fiber mats containing 0.25%, 0.5%, and 1% ciprofloxacin showed inhibition zones against *E. Coli* (≈28 mm) and *S. aureus* (≈20 mm) [72], other studies showing up to 37 mm inhibition [73].

P. aeruginosa and *S. aureus* have a strong natural resistance to many antibiotics, which limits treatment options. Therefore, silver nanoparticles (AgNPs) are being investigated as promising alternatives for preventing and controlling infections [5,6]. Our results show enhanced antimicrobial activity of ciprofloxacin as to what is commonly found in other studies testing the mere antibiotic activity for these strains (around 25-33mm) [74,75]. Our results also show greater antibiotic susceptibility of Gram-negative *P. aueruginosa*, which can be attributed to the thinner peptidoglycan layer as opposed to Gram-positive *S. aureus*, which with a thicker peptidoglycan layer functioning as a barrier against nanoparticles. Moreover, silver ions more easily bind to negatively charged surfaces, such as lipopolysaccharides found in the outer membrane of Gram-negative bacteria. This observation can be explained by the synergistic effect between silver nanoparticles and ciprofloxacin. While ciprofloxacin efficiently penetrates the outer membrane of Gram-negative bacteria, silver nanoparticles can further increase membrane permeability and induce oxidative stress, leading to enhanced bactericidal activity against *P. aeruginosa* compared to *S. aureus*. The differences in antibacterial activity among the composite materials may result from the composition of their matrices; those containing a higher amount of chitosan exhibit slightly increased antibacterial activity, which is consistent with the known properties of chitosan. In the future, it would be valuable to investigate the antimicrobial activity of the solutions after a prolonged period of silver ion release, once the antibiotic has been completely released from the composite. At that point, the composites containing silver ions could potentially retain antimicrobial activity, this time due to the action of the silver ions themselves. As shown in Figure 4, the release of silver ions increases over time, suggesting that such a study could yield highly interesting results. This will be the focus of our upcoming research.

Conclusions

In this study, novel polysaccharide-based composite materials were successfully developed using chitosan and alginate matrices reinforced with sericin and loaded with ciprofloxacin and silver, the latter introduced either as ions within nanocrystalline hydroxyapatite or as silver nanoparticles. The combination of the solid–liquid method with lyophilization enabled the formation of highly porous structures, as confirmed by SEM observations. The composites demonstrated sustained release of both ciprofloxacin and silver species for up to 28 days. Mathematical modeling of the release kinetics revealed a biphasic mechanism for ciprofloxacin and silver ions, initially governed by diffusion through the swollen matrix and subsequently by matrix relaxation and gelation processes. In contrast, silver nanoparticles displayed an increased release in the second phase, following zero-order kinetics.

All silver-containing materials showed pronounced antibacterial activity against *Staphylococcus aureus* (NCTC 9789) and *Pseudomonas aeruginosa* (PAO1161), including multi-drug resistant strains. These results confirm the dual functionality of the composites, which can act simultaneously as temporary bone fillers and localized drug delivery systems, capable of supporting bone tissue regeneration while preventing infection associated with orthopedic implants.

The present findings emphasize the added value of combining polysaccharide matrices with sericin reinforcement and dual antimicrobial agents. Such an approach allows for tunable release profiles and prolonged antimicrobial protection, addressing one of the major clinical challenges in orthopedic and reconstructive surgery—post-implant infections in poorly vascularized tissues.

However, this study has several limitations. Our research aimed to evaluate the synergistic effect of the dual-loaded (silver and ciprofloxacin) composites, rather than to quantify the

independent contribution of each component. We plan to continue the studies focusing on quantifying the synergistic effect between ciprofloxacin and silver nanoparticles. The biological assays were limited to *in vitro* antibacterial evaluation and the mechanical and degradation behavior under physiological conditions was not investigated.

Future research should therefore focus on detailed mechanical testing and *in vivo* evaluation to validate the biological safety and therapeutic performance of the developed composites. Expanding this concept towards multifunctional scaffolds with enhanced osteoinductive and angiogenic properties could further advance their application in bone tissue engineering and localized infection control using such materials as local dressings for bone wounds.

References

[1] E. Kasapgil, M. Garay-Sarmiento, C. Rodriguez-Emmenegger, Advanced Antibacterial Strategies for Combatting Biomaterial-Associated Infections: A Comprehensive Review, WIREs Nanomedicine Nanobiotechnology 16 (2024) e2018. https://doi.org/10.1002/wnan.2018.

[2] N. Blanco-Cabra, J. Alcàcer-Almansa, J. Admella, B.V. Arévalo-Jaimes, E. Torrents, Nanomedicine against biofilm infections: A roadmap of challenges and limitations, WIREs Nanomedicine Nanobiotechnology 16 (2024) e1944. https://doi.org/10.1002/wnan.1944.

[3] N.A. Hodges, E.M. Sussman, J.P. Stegemann, Aseptic and septic prosthetic joint loosening: Impact of biomaterial wear on immune cell function, inflammation, and infection, Biomaterials 278 (2021) 121127.

[4] E. Tacconelli, E. Carrara, A. Savoldi, S. Harbarth, M. Mendelson, D.L. Monnet, C. Pulcini, G. Kahlmeter, J. Kluytmans, Y. Carmeli, Discovery, research, and development of new antibiotics: the WHO priority list of antibiotic-resistant bacteria and tuberculosis, Lancet Infect. Dis. 18 (2018) 318–327.

[5] S. Tang, J. Zheng, Antibacterial Activity of Silver Nanoparticles: Structural Effects, Adv. Healthc. Mater. 7 (2018) 1701503. https://doi.org/10.1002/adhm.201701503.

[6] B. Le Ouay, F. Stellacci, Antibacterial activity of silver nanoparticles: A surface science insight, Nano Today 10 (2015) 339–354.

[7] W.K. Jung, H.C. Koo, K.W. Kim, S. Shin, S.H. Kim, Y.H. Park, Antibacterial Activity and Mechanism of Action of the Silver Ion in *Staphylococcus aureus* and *Escherichia coli*, Appl. Environ. Microbiol. 74 (2008) 2171–2178. https://doi.org/10.1128/AEM.02001-07.

[8] K. Mijnendonckx, N. Leys, J. Mahillon, S. Silver, R. Van Houdt, Antimicrobial silver: uses, toxicity and potential for resistance, BioMetals 26 (2013) 609–621. https://doi.org/10.1007/s10534-013-9645-z.

[9] Q.L. Feng, J. Wu, G.Q. Chen, F.Z. Cui, T.N. Kim, J.O. Kim, A mechanistic study of the antibacterial effect of silver ions onEscherichia coli andStaphylococcus aureus, J. Biomed. Mater. Res. 52 (2000) 662–668. https://doi.org/10.1002/1097-4636(20001215)52:4<662::AID-JBM10>3.0.CO;2-3.

[10] X. Guo, P. Song, F. Li, Q. Yan, Y. Bai, J. He, Q. Che, H. Cao, J. Guo, Z. Su, Research Progress of Design Drugs and Composite Biomaterials in Bone Tissue Engineering, Int. J. Nanomedicine Volume 18 (2023) 3595–3622. https://doi.org/10.2147/IJN.S415666.

[11] S. Mondal, U. Pal, 3D hydroxyapatite scaffold for bone regeneration and local drug delivery applications, J. Drug Deliv. Sci. Technol. 53 (2019) 101131.

[12] V. Mouriño, J.P. Cattalini, J.A. Roether, P. Dubey, I. Roy, A.R. Boccaccini, Composite polymer-bioceramic scaffolds with drug delivery capability for bone tissue engineering, Expert Opin. Drug Deliv. 10 (2013) 1353–1365. https://doi.org/10.1517/17425247.2013.808183.

[13] J. Venkatesan, I. Bhatnagar, P. Manivasagan, K.-H. Kang, S.-K. Kim, Alginate composites for bone tissue engineering: A review, Int. J. Biol. Macromol. 72 (2015) 269–281.

[14] N. Farshidfar, S. Iravani, R.S. Varma, Alginate-based biomaterials in tissue engineering and regenerative medicine, Mar. Drugs 21 (2023) 189.

[15] J. Fourie, F. Taute, L. Du Preez, D. De Beer, Chitosan Composite Biomaterials for Bone Tissue Engineering—a Review, Regen. Eng. Transl. Med. 8 (2022) 1–21. https://doi.org/10.1007/s40883-020-00187-7.

[16] H. Li, F. Jiang, S. Ye, Y. Wu, K. Zhu, D. Wang, Bioactive apatite incorporated alginate microspheres with sustained drug-delivery for bone regeneration application, Mater. Sci. Eng. C 62 (2016) 779–786.

[17] Y. Bi, Z. Lin, S. Deng, Fabrication and characterization of hydroxyapatite/sodium alginate/chitosan composite microspheres for drug delivery and bone tissue engineering, Mater. Sci. Eng. C 100 (2019) 576–583.

[18] Y. Song, Q. Hu, Q. Liu, S. Liu, Y. Wang, H. Zhang, Design and fabrication of drug-loaded alginate/hydroxyapatite/collagen composite scaffolds for repairing infected bone defects, J. Mater. Sci. 58 (2023) 911–926. https://doi.org/10.1007/s10853-022-08053-3.

[19] F. Ordikhani, A. Simchi, Long-term antibiotic delivery by chitosan-based composite coatings with bone regenerative potential, Appl. Surf. Sci. 317 (2014) 56–66.

[20] B. Kołodziejska, R. Figat, J. Kolmas, Biomimetic apatite/natural polymer composite granules as multifunctional dental tissue regenerative material, Int. J. Mol. Sci. 24 (2023) 16751.

[21] I. Arzate-Vázquez, J.J. Chanona-Pérez, G. Calderón-Domínguez, E. Terres-Rojas, V. Garibay-Febles, A. Martínez-Rivas, G.F. Gutiérrez-López, Microstructural characterization of chitosan and alginate films by microscopy techniques and texture image analysis, Carbohydr. Polym. 87 (2012) 289–299.

[22] A.R. Costa-Pinto, R.L. Reis, N.M. Neves, Scaffolds Based Bone Tissue Engineering: The Role of Chitosan, Tissue Eng. Part B Rev. 17 (2011) 331–347. https://doi.org/10.1089/ten.teb.2010.0704.

[23] T.W. Wong, W.H.N.S. Ashikin, C.L. Law, Evaporation and Diffusion Transport Properties and Mechanical Properties of Alginate Dried Film, Dry. Technol. 32 (2014) 117–125. https://doi.org/10.1080/07373937.2013.821479.

[24] K. Baysal, A.Z. Aroguz, Z. Adiguzel, B.M. Baysal, Chitosan/alginate crosslinked hydrogels: Preparation, characterization and application for cell growth purposes, Int. J. Biol. Macromol. 59 (2013) 342–348.

[25] P. Dey, Bone mineralisation, in: Contemp. Top. Phosphorus Biol. Mater., IntechOpen, 2020. https://books.google.com/books?hl=en&lr=&id=TJYtEAAAQBAJ&oi=fnd&pg=PA35&dq=hydroxyapatite+mineralised+tissues&ots=xiKdNlVF5p&sig=kJdvwK43bJmLO0kDKimj9DhJ2SE (accessed May 31, 2025).

[26] R.Z. LeGeros, J.P. LeGeros, Hydroxyapatite, in: Bioceram. Their Clin. Appl., Elsevier, 2008: pp. 367–394. https://www.sciencedirect.com/science/article/pii/B9781845692049500168 (accessed May 31, 2025).

[27] T. Kono, T. Sakae, H. Nakada, T. Kaneda, H. Okada, Confusion between carbonate apatite and biological apatite (carbonated hydroxyapatite) in bone and teeth, Minerals 12 (2022) 170.

[28] J. Wang, L.L. Shaw, Nanocrystalline hydroxyapatite with simultaneous enhancements in hardness and toughness, Biomaterials 30 (2009) 6565–6572.

[29] M.U. Munir, S. Salman, I. Javed, S.N.A. Bukhari, N. Ahmad, N.A. Shad, F. Aziz, Nano-hydroxyapatite as a delivery system: overview and advancements, Artif. Cells Nanomedicine Biotechnol. 49 (2021) 717–727. https://doi.org/10.1080/21691401.2021.2016785.

[30] Y. Li, T. Wu, G. Zhang, A. Fang, Y. Li, S. Wang, H. Yan, P. Liang, J. Lian, Y. Zhang, A native sericin wound dressing spun directly from silkworms enhances wound healing, Colloids Surf. B Biointerfaces 225 (2023) 113228.

[31] S. Baptista-Silva, S. Borges, A.R. Costa-Pinto, R. Costa, M. Amorim, J.R. Dias, Ó. Ramos, P. Alves, P.L. Granja, R. Soares, M. Pintado, A.L. Oliveira, *In Situ* Forming Silk Sericin-Based Hydrogel: A Novel Wound Healing Biomaterial, ACS Biomater. Sci. Eng. 7 (2021) 1573–1586. https://doi.org/10.1021/acsbiomaterials.0c01745.

[32] J. Liu, L. Shi, Y. Deng, M. Zou, B. Cai, Y. Song, Z. Wang, L. Wang, Silk sericin-based materials for biomedical applications, Biomaterials (2022) 121638.

[33] R.I. Kunz, R.M.C. Brancalhão, L.D.F.C. Ribeiro, M.R.M. Natali, Silkworm Sericin: Properties and Biomedical Applications, BioMed Res. Int. 2016 (2016) 1–19. https://doi.org/10.1155/2016/8175701.

[34] P. Aramwit, S. Napavichayanum, P. Pienpinijtham, Y. Rasmi, N. Bang, Antibiofilm activity and cytotoxicity of silk sericin against *Streptococcus mutans* bacteria in biofilm: an *in vitro* study, J. Wound Care 29 (2020) S25–S35. https://doi.org/10.12968/jowc.2020.29.Sup4.S25.

[35] P. Ghensi, E. Bettio, D. Maniglio, E. Bonomi, F. Piccoli, S. Gross, P. Caciagli, N. Segata, G. Nollo, F. Tessarolo, Dental implants with anti-biofilm properties: a pilot study for developing a new sericin-based coating, Materials 12 (2019) 2429.

[36] G.T. Hailu, M.T. Alemea, F. Lemessa, Development of silk sericin-based polysaccharide-protein hybrid biofilms: Mechanical, thermal, and antibacterial properties, Res. 2 (2025) 100097.

[37] S. Sunarintyas, W. Siswomihardjo, The effect of sericin application over hydroxyapatite surface on osteoblast cells proliferation, in: 2011 2nd Int. Conf. Instrum. Commun. Inf. Technol. Biomed. Eng., IEEE, 2011: pp. 145–149. https://ieeexplore.ieee.org/abstract/document/6108613/ (accessed May 31, 2025).

[38] C. Noosak, P. Jantorn, J. Meesane, S. Voravuthikunchai, D. Saeloh, Dual-functional bioactive silk sericin for osteoblast responses and osteomyelitis treatment, PLoS One 17 (2022) e0264795.

[39] S. Nayak, T. Dey, D. Naskar, S.C. Kundu, The promotion of osseointegration of titanium surfaces by coating with silk protein sericin, Biomaterials 34 (2013) 2855–2864.

[40] M. Jiang, S. Li, P. Ming, Y. Guo, L. Yuan, X. Jiang, Y. Liu, J. Chen, D. Xia, Y. He, G. Tao, Rational design of porous structure-based sodium alginate/chitosan sponges loaded with green synthesized hybrid antibacterial agents for infected wound healing, Int. J. Biol. Macromol. 237 (2023) 123944. https://doi.org/10.1016/j.ijbiomac.2023.123944.

[41] A. Kyzioł, A. Mazgała, J. Michna, A. Regiel-Futyra, V. Sebastian, Preparation and characterization of alginate/chitosan formulations for ciprofloxacin-controlled delivery, J. Biomater. Appl. 32 (2017) 162–174. https://doi.org/10.1177/0885328217714352.

[42] Q. Ma, S. Salathia, M.R. Gigliobianco, C. Casadidio, P. Di Martino, R. Censi, Recent Insights into the Potential and Challenges of Sericin as a Drug Delivery Platform for Multiple Biomedical Applications, Pharmaceutics 17 (2025) 695. https://doi.org/10.3390/pharmaceutics17060695.

[43] C. Noosak, K. Iamthanaporn, J. Meesane, S.P. Voravuthikunchai, D.S. Sotthibandhu, Bioactive functional sericin/polyvinyl alcohol hydrogel: biomaterials for supporting orthopedic surgery in osteomyelitis, J. Mater. Sci. 58 (2023) 5477–5488. https://doi.org/10.1007/s10853-023-08356-z.

[44] K. Pajor, Ł. Pajchel, A. Zgadzaj, U. Piotrowska, J. Kolmas, Modifications of hydroxyapatite by gallium and silver ions—physicochemical characterization, cytotoxicity and antibacterial evaluation, Int. J. Mol. Sci. 21 (2020) 5006.

[45] A. Luanda, M. Mahadev, R.N. Charyulu, V. Badalamoole, Evaluation of Dual Drug Delivery Efficiency of Nanocomposite Hydrogel Containing Pectin for Combating Cancer, Polym. Adv. Technol. 36 (2025) e70118. https://doi.org/10.1002/pat.70118.

[46] C. Corsaro, G. Neri, A.M. Mezzasalma, E. Fazio, Weibull Modeling of Controlled Drug Release from Ag-PMA Nanosystems, Polymers 13 (2021) 2897. https://doi.org/10.3390/polym13172897.

[47] B. Iso, B. STANDARD, Biological evaluation of medical devices, Part 1 (2009) 10993.

[48] A. Luanda, M. Mahadev, R.N. Charyulu, V. Badalamoole, Locust bean gum-based silver nanocomposite hydrogel as a drug delivery system and an antibacterial agent, Int. J. Biol. Macromol. 282 (2024) 137097. https://doi.org/10.1016/j.ijbiomac.2024.137097.

[49] R. Varma, S. Vasudevan, Extraction, Characterization, and Antimicrobial Activity of Chitosan from Horse Mussel *Modiolus modiolus*, ACS Omega 5 (2020) 20224–20230. https://doi.org/10.1021/acsomega.0c01903.

[50] Z.Z. Zam, F. Muin, A. Fataruba, Identification of chitosan beads from coconut crab patani variety using Fourier Transform Infrared Spectroscopy (FTIR), in: J. Phys. Conf. Ser., IOP Publishing, 2021: p. 012014. https://iopscience.iop.org/article/10.1088/1742-6596/1832/1/012014/meta (accessed July 29, 2025).

[51] D. Leal, B. Matsuhiro, M. Rossi, F. Caruso, FT-IR spectra of alginic acid block fractions in three species of brown seaweeds, Carbohydr. Res. 343 (2008) 308–316.

[52] Z. Belattmania, S. Kaidi, S. El Atouani, C. Katif, F. Bentiss, C. Jama, A. Reani, B. Sabour, V. Vasconcelos, Isolation and FTIR-ATR and 1H NMR characterization of alginates from the main alginophyte species of the atlantic coast of Morocco, Molecules 25 (2020) 4335.

[53] S. Sahoo, C.K. Chakraborti, S. Naik, S.C. Mishra, U.N. Nanda, Structural analysis of ciprofloxacin-carbopol polymeric composites by X-Ray diffraction and Fourier transform infra-red spectroscopy, Trop. J. Pharm. Res. 10 (2011). https://www.ajol.info/index.php/tjpr/article/view/67938/0 (accessed July 29, 2025).

[54] S. Durgapal, S. Mukhopadhyay, L. Goswami, Preparation, characterization and evaluation of floating microparticles of ciprofloxacin, Int J Appl Pharm 9 (2017) 1–8.

[55] A.W. Chan, R.J. Neufeld, Modeling the controllable pH-responsive swelling and pore size of networked alginate based biomaterials, Biomaterials 30 (2009) 6119–6129.

[56] G. Pasparakis, N. Bouropoulos, Swelling studies and in vitro release of verapamil from calcium alginate and calcium alginate–chitosan beads, Int. J. Pharm. 323 (2006) 34–42. https://doi.org/10.1016/j.ijpharm.2006.05.054.

[57] V. Uskoković, Mechanism of formation governs the mechanism of release of antibiotics from calcium phosphate nanopowders and cements in a drug-dependent manner, J. Mater. Chem. B 7 (2019) 3982–3992.

[58] M. Fosca, J.V. Rau, V. Uskoković, Factors influencing the drug release from calcium phosphate cements, Bioact. Mater. 7 (2022) 341–363.

[59] N.S. Heredia, K. Vizuete, M. Flores-Calero, K. Pazmiño V, F. Pilaquinga, B. Kumar, A. Debut, Comparative statistical analysis of the release kinetics models for nanoprecipitated drug delivery systems based on poly (lactic-co-glycolic acid), PLoS One 17 (2022) e0264825.

[60] S. Dash, P.N. Murthy, L. Nath, P. Chowdhury, Kinetic modeling on drug release from controlled drug delivery systems, Acta Pol Pharm 67 (2010) 217–223.

[61] L.P. Jahromi, M. Ghazali, H. Ashrafi, A. Azadi, A comparison of models for the analysis of the kinetics of drug release from PLGA-based nanoparticles, Heliyon 6 (2020). https://www.cell.com/heliyon/fulltext/S2405-8440(20)30296-6 (accessed April 29, 2025).

[62] Y. Fu, W.J. Kao, Drug release kinetics and transport mechanisms of non-degradable and degradable polymeric delivery systems, Expert Opin. Drug Deliv. 7 (2010) 429–444. https://doi.org/10.1517/17425241003602259.

[63] J. Kolmas, P. Romaniuk, D. Predoi, A. Drobniewska, K. Burdan, B. Kołodziejska, Magnesium ion substitution in various calcium phosphates: A way towards bone regeneration, Ceram. Int. 51 (2025) 1153–1160.

[64] A.S. Abdul Rahman, A.N.S. Fizal, N.A. Khalil, A.N. Ahmad Yahaya, M.S. Hossain, M. Zulkifli, Fabrication and characterization of magnetic cellulose–chitosan–alginate composite hydrogel bead bio-sorbent, Polymers 15 (2023) 2494.

[65] W.L. Guerra-Ponce, S.L. Gracia-Vásquez, P. González-Barranco, I.A. Camacho-Mora, Y.A. Gracia-Vásquez, E. Orozco-Beltrán, L.A. Felton, In vitro evaluation of sustained released matrix tablets containing ibuprofen: a model poorly water-soluble drug, Braz. J. Pharm. Sci. 52 (2016) 751–759.

[66] K. Sinulingga, M. Sirait, N. Siregar, M.E. Doloksaribu, Investigation of Antibacterial Activity and Cell Viability of Ag/Mg and Ag/Zn Co-doped Hydroxyapatite Derived from Natural Limestone, ACS Omega 6 (2021) 34185–34191. https://doi.org/10.1021/acsomega.1c05921.

[67] K. Pajor, A. Michalicha, A. Belcarz, L. Pajchel, A. Zgadzaj, F. Wojas, J. Kolmas, Antibacterial and cytotoxicity evaluation of new hydroxyapatite-based granules containing silver or gallium ions with potential use as bone substitutes, Int. J. Mol. Sci. 23 (2022) 7102.

[68] F. Afhkami, P. Ahmadi, G. Rostami, Cytotoxicity of Different Concentrations of Silver Nanoparticles and Calcium Hydroxide for MC3T3-E1 Preosteoblast Cell Line, Clin. Exp. Dent. Res. 11 (2025) e70075. https://doi.org/10.1002/cre2.70075.

[69] L.S. Daniel, M.T. Joseph, V. Uahengo, M. Hedimbi, Antibacterial Activity of Visible Light Responsive-Silver-Nanoparticle/Titania Composite Thin Films with Unprecedently Higher Amounts of Silver, Adv. Mater. Interfaces 11 (2024) 2400035. https://doi.org/10.1002/admi.202400035.

[70] R. Cao, X. Zhai, X. Li, X. Zhao, Antibacterial properties of a novel nano-silver loaded poly(styrene-co-acrylic) composites, Polym. Polym. Compos. (2021). https://doi.org/10.1177/09673911211037499.

[71] M. Ghavam, Antibacterial potential of biosynthesized silver nanoparticles using Nepeta sessilifolia Bunge and Salvia hydrangea DC. ex Benth. extracts from the natural habitats of Iran's Rangelands, BMC Complement. Med. Ther. 23 (2023) 299. https://doi.org/10.1186/s12906-023-04101-w.

[72] M.A. Obeid, L. Akil, A.A. Aljabali, I. Khadra, Characterization of Ciprofloxacin-Loaded Polymeric Fiber Mats Prepared by Melt Electrospinning, Macromol. Mater. Eng. 309 (2024) 2300376. https://doi.org/10.1002/mame.202300376.

[73] M. Pahlevani, M. Beig, S.M. Barzi, M. Sadeghzadeh, M. Shafiei, M. Chiani, A. Sohrabi, M. Sholeh, S. Nasr, Antibacterial and wound healing effects of PEG-coated ciprofloxacin-loaded ZIF-8 nanozymes against ciprofloxacin-resistant Pseudomonas aeruginosa taken from burn wounds, Front. Pharmacol. 16 (2025). https://doi.org/10.3389/fphar.2025.1556335.

[74] M. Abu-Sini, M.A. Al-Kafaween, R.M. Al-Groom, A.B.M. Hilmi, M. Abu-Sini, M.A. Al-Kafaween, R.M. Al-Groom, A.B.M. Hilmi, Comparative *in vitro* activity of various antibiotic against planktonic and biofilm and the gene expression profile in *Pseudomonas*

aeruginosa, AIMS Microbiol. 9 (2023) 313–331. https://doi.org/10.3934/microbiol.2023017.

[75] M.M. Masadeh, K.H. Alzoubi, W.S. Ahmed, A.S. Magaji, In Vitro Comparison of Antibacterial and Antibiofilm Activities of Selected Fluoroquinolones against Pseudomonas aeruginosa and Methicillin-Resistant Staphylococcus aureus, Pathogens 8 (2019) 12. https://doi.org/10.3390/pathogens8010012.

Funding: This work was supported by the Medical University of Warsaw (WF6/N/25).

Captions:

Figure 1. SEM images of all obtained composites.

Figure 2. Swelling test. The graph shows the swelling ratio (%) of the obtained materials at different times.

Figure 3. Ciprofloxacin release profiles from the composite matrices: full release curves over 672 hours (a), initial release phase - first 48 hours (b); representative model fittings to Korsmeyer-Peppas model for C3AgHA in the short- and long-term release ranges (c, d – respectively).

Figure 4. Silver release profiles from all composite matrices (a), model fitting results for materials with silver-ion-doped hydroxyapatite (b–c), fitted release curves for composites containing hydroxyapatite with embedded silver nanoparticles (d–e).

Figure 1. SEM images of all obtained composites.

Click here to access/download;Figure;Figure1,corr.jpg

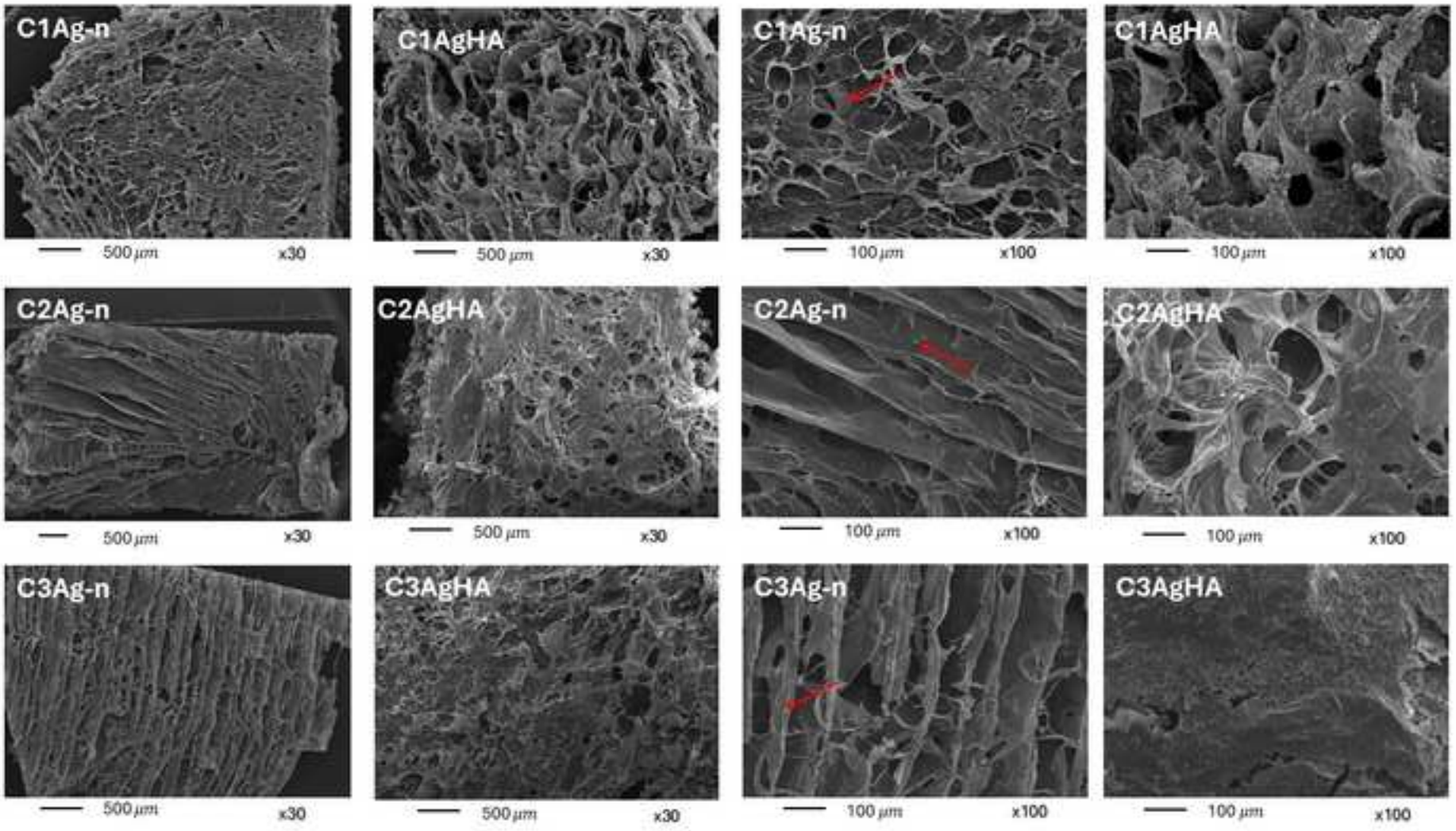

Figure 2. Swelling test. The graph shows the swelling ratio (%) of the obtained materials at different times.

Click here to access/download;Figure;Swelling Figure.TIF

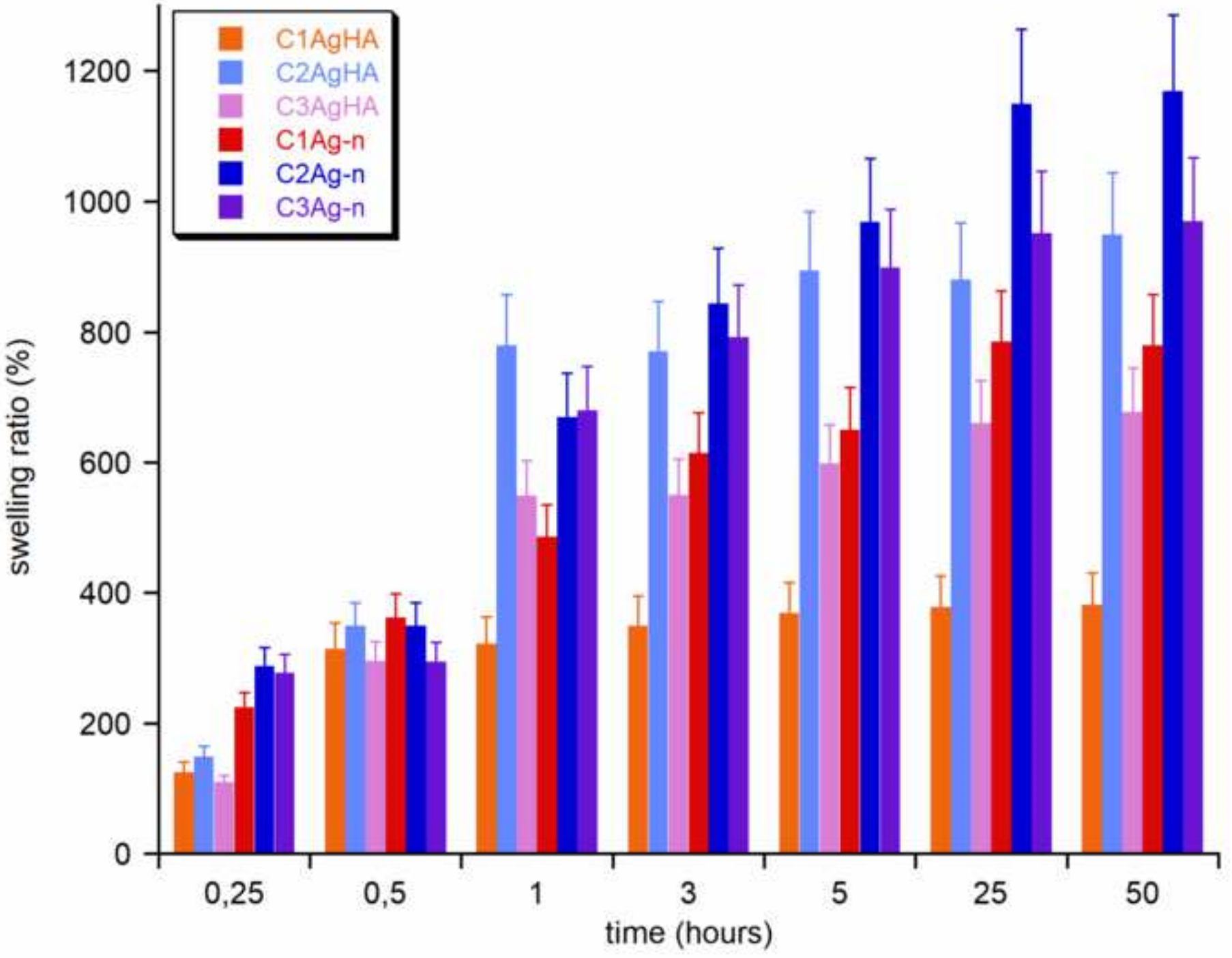

Figure 3. Ciprofloxacin release profiles from the composite matrices: full release curves over 672 hours (a), initial release phase - first 48 hours (b); representative model

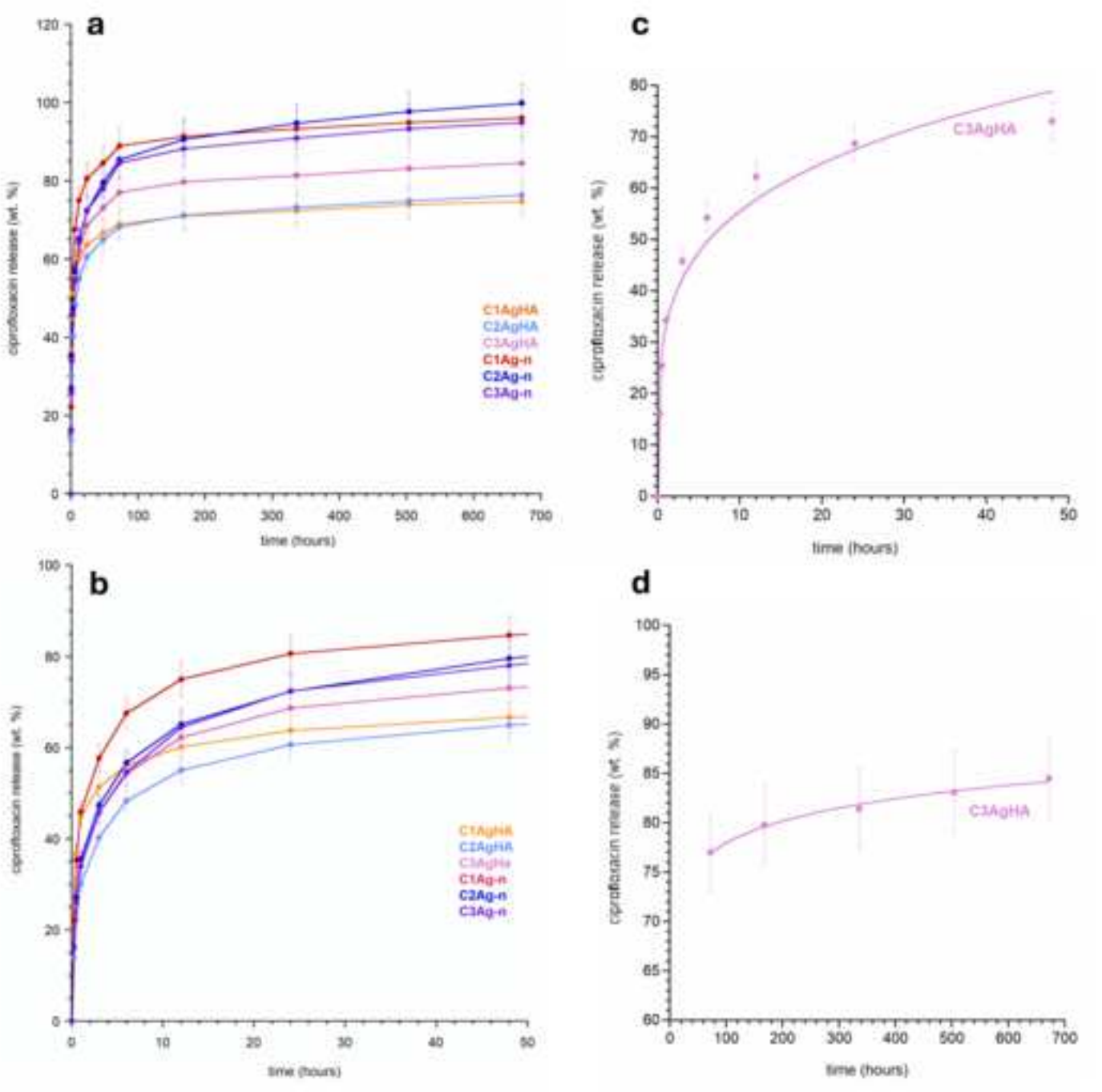

Figure 4. Silver release profiles from all composite matrices (a), model fitting results for materials with silver-ion-doped

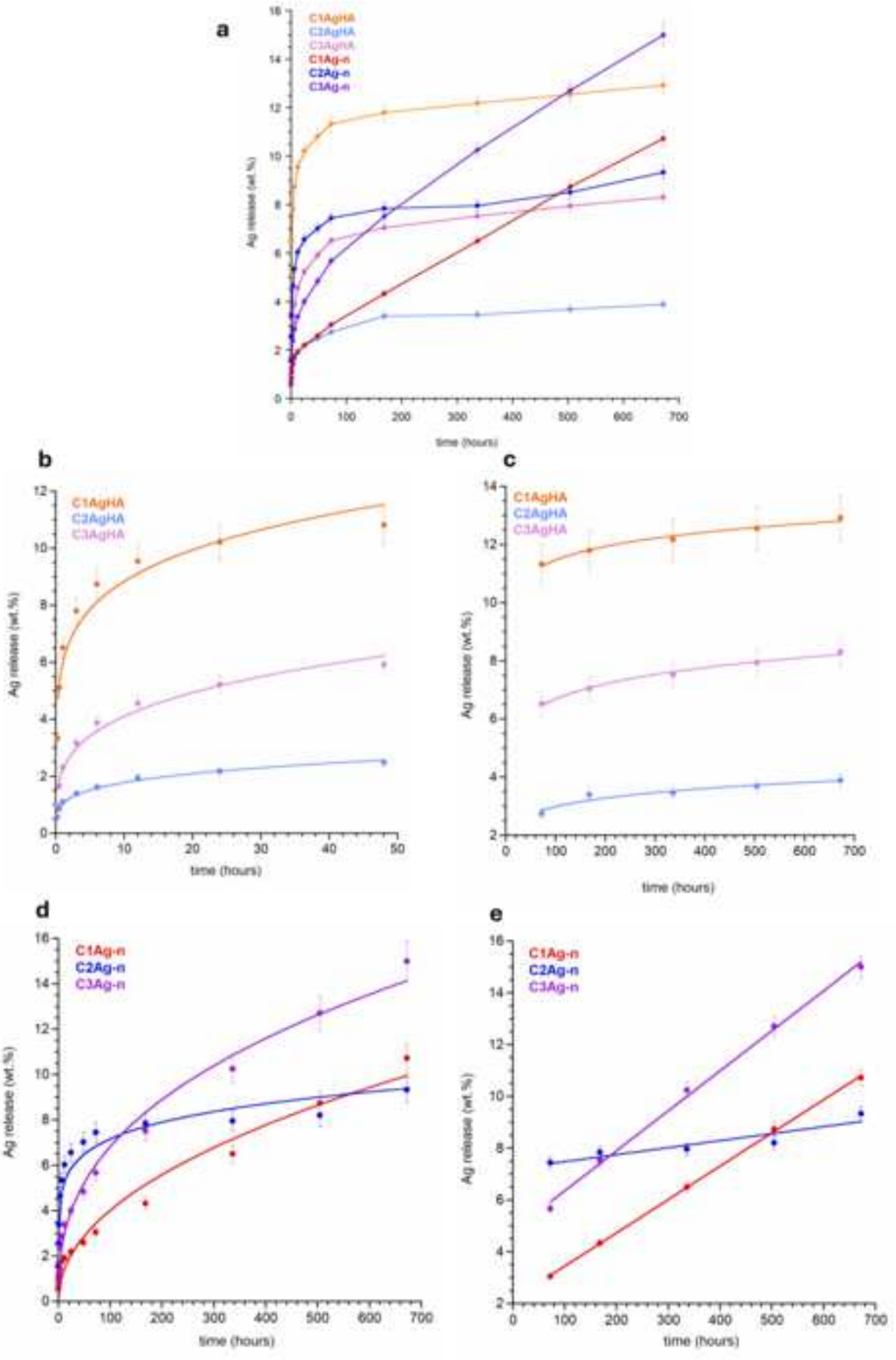

Declaration of interests

☒The authors declare that they have no known competing financial interests or personal relationships that could have appeared to influence the work reported in this paper.

☐The authors declare the following financial interests/personal relationships which may be considered as potential competing interests:

CRediT author statement:

Barbara Kołodziejska: Conceptualization, Methodology, Investigation, Writing- Original draft preparation, Writing- Reviewing and Editing; **Andrzej Pyzik**: Investigation; **Ramona Figat**: Investigation; **Julia Kopczyńska**: Investigation; **Magdalena Kowalczyk**: Investigation; **Joanna Kolmas**: Conceptualization, Methodology, Writing- Original draft preparation, Writing- Reviewing and Editing, Supervision